AD-A160 828 A CASE STUDY OF A MID-ATLANTIC COASTAL FRONT(U) AIR FORCE INST OF TECH WRIGHT-PATTERSON AFB OH J T KROLL 1985 AFIT/CI/NR-85-135T 1/2

UNCLASSIFIED F/G 4/1 NL

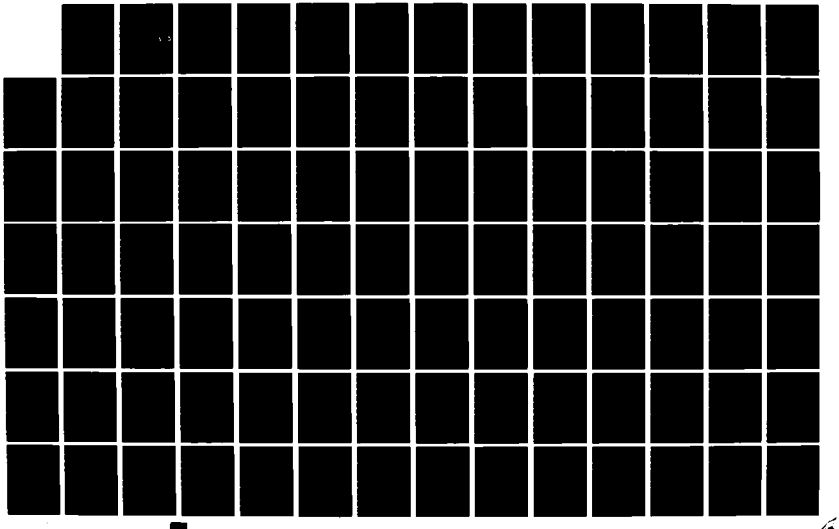

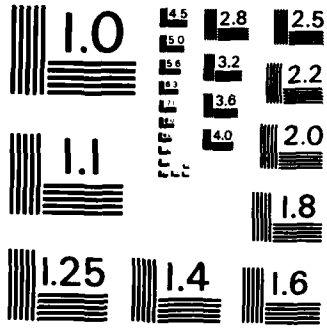


MICROCOPY RESOLUTION TEST CHART
NATIONAL BUREAU OF STANDARDS - 1963 - A

UNCLASS

SECURITY CLASSIFICATION OF THIS PAGE (When Data Entered)

(1)

## REPORT DOCUMENTATION PAGE

READ INSTRUCTIONS BEFORE COMPLETING FORM

| | |
|---|---|
| 1. REPORT NUMBER: AFIT/CI/NR 85- 135T | 2. GOVT ACCESSION NO: AD-A160 828 |
| 3. RECIPIENT'S CATALOG NUMBER: | |
| 4. TITLE (and Subtitle): A Case Study Of A Mid-Atlantic Coastal Front | 5. TYPE OF REPORT & PERIOD COVERED: THESIS/DISSERTATION |
| | 6. PERFORMING ORG. REPORT NUMBER: |
| 7. AUTHOR(s): James T. Kroll | 8. CONTRACT OR GRANT NUMBER(s): |
| 9. PERFORMING ORGANIZATION NAME AND ADDRESS: AFIT STUDENT AT: North Carolina State University | 10. PROGRAM ELEMENT, PROJECT, TASK AREA & WORK UNIT NUMBERS: |
| 11. CONTROLLING OFFICE NAME AND ADDRESS: AFIT/NR, WPAFB OH 45433 - 6583 | 12. REPORT DATE: 1985 |
| | 13. NUMBER OF PAGES: 90 |
| 14. MONITORING AGENCY NAME & ADDRESS(if different from Controlling Office) | 15. SECURITY CLASS. (of this report): UNCLASS |
| | 15a. DECLASSIFICATION/DOWNGRADING SCHEDULE: |

16. DISTRIBUTION STATEMENT (of this Report)

APPROVED FOR PUBLIC RELEASE; DISTRIBUTION UNLIMITED

DTIC ELECTE S NOV 4 1985 D B

17. DISTRIBUTION STATEMENT (of the abstract entered in Block 20, if different from Report)

18. SUPPLEMENTARY NOTES

APPROVED FOR PUBLIC RELEASE: IAW AFR 190-1

Lynn Wolaver 25 Oct 85

LYNN E. WOLAVER
Dean for Research and
Professional Development
AFIT, Wright-Patterson AFB

19. KEY WORDS (Continue on reverse side if necessary and identify by block number)

20. ABSTRACT (Continue on reverse side if necessary and identify by block number)

ATTACHED

AD-A160 828

DTIC FILE COPY

DD FORM 1 JAN 73 1473 EDITION OF 1 NOV 65 IS OBSOLETE

UNCLASS

SECURITY CLASSIFICATION OF THIS PAGE (When Data Entered)

85 11 04 071

# ABSTRACT

KROLL, JAMES T. A Case Study of a Mid-Atlantic Coastal Front.(Under the direction of DAVID BARBER and GERALD WATSON).

A unique case of mid-Atlantic coastal frontogenesis on December 21-22, 1983 is examined to determine the evolution of the three dimensional structure of this mesoscale phenomena. Analysis of synoptic and mesoscale surface maps suggest a coastal front which moves steadily inland. However, review of temperature and wind profiles at individual stations reveals that frontogenesis actually occurs over the land in North Carolina and southern Virginia. Lagrangian and Eulerian frontogenesis calculations confirm this finding. The frontogenesis process is found to be largely a result of the ageostrophic flow within the cold wedge which results in weak cold air advection over the land. This northerly flow combines with a strong southerly flow over the Atlantic to increase the temperature gradient near the coastline.

Analysis of kinematic variables indicates regions of relatively strong convergence and cyclonic vorticity in the region of the coastal front. Geostrophic deformation maxima

coincide with the ridge of the anticyclonic bulge east of the Appalachians. Three-dimensional Lagrangian frontogenesis computations identify the "shear" and "confluence" terms as frontogenetical within the frontal zone. The "tilting" term is frontolytical within the frontal zone. Precipitation analyses identify the cold air side of the coastal front as favorable for enhanced precipitation. Relationships between preciptation bands and convective instability are also discussed.

To test the hypothesis that the inland ageostrophic flow is a result of problems with the reduction of pressures to sea level, a terrain level geostrophic wind is used to predict wind flow. The terrain level winds failed to produce a better estimate of actual winds than that of the sea level geostrophic winds.

ABSTRACT

A CASE STUDY OF A MID-ATLANTIC COASTAL FRONT

BY

CAPTAIN JAMES T. KROLL

UNITED STATES AIR FORCE

AIR WEATHER SERVICE BRANCH

NORTH CAROLINA STATE UNIVERSITY

1985

MASTERS OF SCIENCE DEGREE

90 PAGES

# A CASE STUDY OF A

# MID-ATLANTIC COASTAL FRONT

by

James T. Kroll

A thesis submitted to the Graduate Faculty of
North Carolina State University
in partial fulfillment of the
requirements for the Degree of
Masters of Science

Department of
Marine, Earth and Atmospheric Sciences

Raleigh
1 9 8 5

APPROVED BY:

Arthur Laman — David A. Barber

Larry A. Nelson — G. T. Csanady
Chairman of Advisory Committee

ABSTRACT

KROLL, JAMES T. A Case Study of a Mid-Atlantic Coastal Front.(Under the direction of DAVID BARBER and GERALD WATSON).

A unique case of mid-Atlantic coastal frontogenesis on December 21-22, 1983 is examined to determine the evolution of the three dimensional structure of this mesoscale phenomena. Analysis of synoptic and mesoscale surface maps suggest a coastal front which moves steadily inland. However, review of temperature and wind profiles at individual stations reveals that frontogenesis actually occurs over the land in North Carolina and southern Virginia. Lagrangian and Eulerian frontogenesis calculations confirm this finding. The frontogenesis process is found to be largely a result of the ageostrophic flow within the cold wedge which results in weak cold air advection over the land. This northerly flow combines with a strong southerly flow over the Atlantic to increase the temperature gradient near the coastline.

Analysis of kinematic variables indicates regions of relatively strong convergence and cyclonic vorticity in the region of the coastal front. Geostrophic deformation maxima coincide with the ridge of the anticyclonic bulge east of the Appalachians. Three-dimensional Lagrangian frontogenesis computations identify the "shear" and

"confluence" terms as frontogenetical within the frontal zone. The "tilting" term is frontolytical within the frontal zone. Precipitation analyses identify the cold air side of the coastal front as favorable for enhanced precipitation. Relationships between preciptation bands and convective instability are also discussed.

To test the hypothesis that the inland ageostrophic flow is a result of problems with the reduction of pressures to sea level, a terrain level geostrophic wind is used to predict wind flow. The terrain level winds failed to produce a better estimate of actual winds than that of the sea level geostrophic winds.

# BIOGRAPHY

James T. Kroll was born in Warren, New Jersey on March 3, 1958. He was raised in that community and graduated from Watchung Hills Regional High School in 1976. He received his Bachelor of Science in Meteorology from Rutgers University in May 1980. In September 1980, he attended the United States Air Force Officer Training School and was commissioned as a Second Lieutenant on December 11, 1980.

The author served as an Assistant Staff Weather Officer to the Third U.S. Army Corps and as the Staff Weather Officer to the Sixth Cavalry Brigade Air Combat while assigned to Detachment 14, 5th Weather Squadron at Fort Hood, Texas. In August 1983, he entered the Graduate School of North Carolina State University and began his studies toward a Masters of Science degree in Meteorology.

The author is married to the former Kristie Ann Olson of Warren, New Jersey. The authors mother, Mrs. Mabel Kroll, currently resides in Middlesex, New Jersey.

# ACKNOWLEDGEMENTS

The author desires to express his appreciation to the United States Air Force and, in particular, the AIr Force Institute of Technology and Air Weather Service for their financial and moral support. He also extends his appreciation to Dr. Gerald Watson, Chairman of the Advisory Committee, and Dr. Dave Barber for sharing their time, knowledge and guidance in preparing this thesis. Appreciation is also extended to Dr. Sethuraman and Dr. Larry Nelson for their assistance.

Particular thanks are given to Raymond Kiess for his aid in computer programming and to Capt. Robert Blevins and Capt. Dewey Harms for their scholastic and personal support during the past two years. Finally, the author wishes to express his utmost appreciation to his wife, Kristie, for her support during the course of study.

TABLE OF CONTENTS

# 1. INTRODUCTION

## 1.1 General Comments

In the colder months of the year, the synoptic pattern over the Eastern United States frequently enhances the development of two mesoscale phenomena, namely, the cold wedge and the coastal front. The cold wedge, also known as the "Appalachian damming effect," is the damming or trapping of a shallow layer of relatively cold air east of the Appalachian mountains. The coastal front is an intense mesoscale baroclinic zone that develops over the relatively warm adjacent coastal waters.

The synoptic pattern responsible for these mesoscale events is dominated by a cold anticyclone centered over New England or southeastern Canada. A striking feature which develops within the cold wedge is the maintenance of northerly flow over the inland region, east of the mountain range. This flow is contrary to what is expected by the analyzed pressure pattern. This ageostrophy is especially pronounced along the base of the mountain range where surface wind direction occasionally differ from the geostrophic direction by more than 90 degrees.

Previous studies indicate that the ageostrophic flow within the cold wedge appears to be a significant factor in developing and maintaining the coastal front. While northeasterly flow dominates inland, the flow over the ocean gradually shifts to the southeast. The coastal front

develops in the boundary zone between the opposing flows. Frontal development is enhanced as the air over the Atlantic traverses long fetches of warmer ocean waters causing temperature modification by sensible heating. This ultimatly results is an increase of the overall onshore-offshore temperature gradient.

The occurrence of these phenomena is significant to the synoptician. Freezing rain is frequently associated with these events during the winter months. The coastal front itself is often the dividing line between frozen and liquid precipitation. Considering that the frontal temperature gradient may be as great as 1 K/Km over a 20-30 Km wide zone, the prediction of frozen versus non-frozen precipitation regions is difficult. Adding to the dilemma is the inability of the operational forecast models to handle correctly this boundary layer phenomena. The forecast models tend to eliminate the high pressure wedge and establish a warming trend over the coastal regions. This rarely occurs.

Bosart(1972) identified New England and the Carolinas as two geographical regions with a marked preference for coastal front development. Bosart and Korty(1976) linked the Carolina coastal front with the redevelopment of cyclones moving norhteastward from the Gulf of Mexico. To date, however, detailed analyses of coastal fronts are limited to one analysis in each of these preferred regions.

## 1.2 Objectives

As a preliminary study of the East Coast Cyclone Project (GALE), this research presents a case study to illustrate a mid-Atlantic coastal front event. Efforts concentrate on depicting the surface and three-dimensional structure of the coastal front as well as identifying the processes which affect frontal evolution. Specifically, an objective analysis scheme is used to derive pertinent meteorological parameters (i.e. divergence, gradients, advections, etc.). Eulerian and Lagrangian forms of the frontogenesis equation are also applied. Relationships between these results and frontal evolution and movement are established.

The relationships between frontal structure and weather distibution are also examined. Potential instability analyses are examined in conjunction with the precipitation distribution. In addition, terrain-level geostrophic winds are compared with geostrophic winds based upon pressures reduced to sea level as an alternative to predicting wind flow within the cold wedge.

The selected case is not associated with any marked cyclogenesis. The event is a moderately intense coastal front which passes through reporting stations 80-120 Km inland. Because the frontal zone passes through a dense network of surface reporting stations, a more complete analysis of frontal evolution may be obtained.

## 1.3 Literature Review

### 1.3.1 General Frontal Studies

J. Bjerknes(1919) is generally credited with documenting the first significant description of surface front structures and the relationship to extratropical cyclones. He noted two lines of convergence intersecting at the cyclone center which bounded the warm air region. Bjerkes and Solberg(1922) elaborated upon the cyclone model to include its entire life cycle. According to the theory, the polar front was a zero-order discontinuity in density or temperature which intersected the earth's surface.

With the advent of upper air soundings, Bjerknes(1932) discovered first-order discontinuities in the upper level frontal boundaries. Instead of sharp contrasts in temperature, he discovered a sharp contrast in temperature gradients. This led to the concept of fronts as zones of transition and not lines of abrupt change.

Petterssen(1940) extensively discussed frontogenesis in relationship to wind fields. The concept of frontogenesis involves the juxtaposition of two differing air masses leading to the creation of a discontinuity in the temperature field. Defining "frontogenesis" as

$$F = (\partial/\partial t)|\nabla S| \ , \qquad 1.1$$

where $VS$ is the magnitude of the gradient of a

conservative property S, frontogenesis occurs where the gradient of S increases most rapidly. Petterssen displays deformative, divergent and rotational fields in relation to frontogenesis. He concludes that deformative fields are frontogenetical when the isotherms lie within a 45 degree angle of the axis of dilatation. Isotherms lying at a larger angle to this axis make the deformative field frontolytical. In addition, he resolved the inherent frontogenetical property of a field of convergence and determined that pure rotational fields were neither frontogenetical nor frontolytical.

Prior to this time, frontogenesis concepts were limited to the horizontal plane. Vertical motions in the vicinity of surface fronts, except for forced upslope or downslope, were assumed to be negligible. The expanding network of upper-level soundings provided the opportunity forfrontal analysis at upper levels as well as derived values of vertical motion in the atmosphere. Miller(1948) altered the concepts of frontogenesis when he redefined it as

$$F = d|\nabla S|/dt \qquad 1.2$$

In addition to extending the frontogenetical concepts into three dimensions, Miller's equation also viewed frontogenesis from the parcel following perspective. This perspective has dominated frontal analysis literature since that time.

Palmen(1948) illustrated the temperature and wind

distributions in the vicinity of the polar front. The polar front was identified as a region of strong stability with an associated wind maximum at upper-levels. An extension of this work by Palmen and Newton(1948) verified the existence of a jet stream above the frontal layer in the vicinity of the tropopause. The polar front itself had a varying slope of 1/120 at 500mb compared to 1/175 near the earth's surface. In addition, the mean horizontal wind shear was cyclonic throughout the entire frontal zone with a distinct region of divergence at the southern edge of the jet stream.

Miller's concept of three-dimensional frontogenesis was applied at the 500mb level by Reed and Sanders(1953) and again by Reed(1955). Results indicated that the horizontal gradient of vertical motions (referred to as the "tilting" term) was primarily responsible for frontogenesis at that level. Strong upper-level subsidence at the warm air side of the front was largely responsible for the dominance of that term.

Applying the same concepts, Newton(1954) evaluated factors affecting frontogenesis at multiple levels in the atmosphere. He demonstrated that factors affecting frontogenesis varied at different atmospheric levels. The "tilting" term was a significant frontogenetic factor at mid-levels as was determined by Reed and Sanders. On the contrary, divergence and thermal advection within deformation fields dominated frontogenetic effects at the

surface and at the level of maximum winds. Newton suggested that vertical motions near the surface are damped enough such that their effect on surface frontogenesis was negligible. Also, surface frontogenesis was usually associated with increased vorticity and vorticity changes were affected by divergence and friction. These concepts had been hypothesized earlier by Petterssen and Austin(1942).

The processes of intense surface frontogenesis were investigated by Sanders(1955). Vertical cross sections of the "confluence" and "tilting" terms of Miller's frontogenesis equations were developed. These patterns indicated that the "confluence" term was highly frontogenetical within the frontal zone near the surface (probably due to the extreme confluence and temperature gradients occurring at the surface). On the other hand, the "tilting" term displayed high frontogenetical values in the warm air adjacent to the front while the effect was frontolytical in the frontal zone. The net effect of both terms yielded high frontogenetical quantities within the frontal zone below 1000 feet as well as in the warm air adjacent to the front. High frontolytical values were found in the frontal zone above 1000 feet where the "tilting" term dominated the "confluence" term.

### 1.3.2 Coastal Frontogenesis Studies

The term "coastal frontogenesis" was first used by

Bosart(1972), however, many years earlier the coastal front concept was explored in relation to stratus development in the southeast United States. Carson(1950) analyzed three cases of "Gulf Stream frontogenesis" where a surface warm front developed in the vicinity of the Gulf Stream's central axis. Carson noted the synoptic pattern was typically dominated by a cold core high pressure wedge and that the isobars along the Atlantic Coastal Plain were oriented parallel to the Gulf Stream axis. West of the warm front, winds were northerly with much cooler temperatures while wind on the other side were more easterly. Available soundings indicated that air over the land at 1000-2000 feet was 10-15 K warmer than at the surface.

Carson's studies indicated a systematic increase of the stratus layer tops. The stratus layer initiated at the warm front and sloped upward toward the coast. He suggested the stratus layer was representative of the slope of the cold wedge. Carson hypothesized that air flowing over the warmer ocean waters was lifted and carried westward by the prevailing winds aloft. The strong frontal inversion trapped the lifted air making it possible for stratus to form and develop downward as a result of evaporating precipitation.

Bosart(1972) was credited with the first extensive mesoscale analysis of a coastal front. Special attention was given to the 24 December 1970 case along the New England

coast. Analyses revealed temperature gradients as great as 1 K/Km. The front separated a stronger,easterly and more geostrophic flow over the ocean from a lighter northerly flow over land. He also discovered a tendency for frontal stagnation along the Boston-Providence line as well as a precipitation maximum just west of the frontal zone.

Bosart sites geography, friction, land-sea thermal contrast and latent and sensible heating as the causitive factors of frontogenesis. Using Petterssen's(1956) development equation, he argues that the geography of New England as well as the Carolinas and Texas are favorable for this type of frontogenesis because of the natural tendency for development of the appropriate vorticity. In addition, he concludes that the axis of maximum precipitation is consistent with the quasi-geostrophic omega equation since the axis is within the region of maximum lower tropospheric warm air advection.

As an extension of this study, Bosart(1975) used the same case to analyze the effects of geostrophic versus observed deformation. Analyses indicated that the magnitude of observed deformation surpassed its geostrophic counterpart. Observed deformation fields aligned well with the frontogenesis region while the geostrophic fields displayed a preference for the axis of the anticyclonic wedge. Also, the angle of the isotherms to the geostrophic deformation axis of dilatation far exceeded the critical 45

degrees necessary for frontogenesis. He concluded that geostrophic deformation was not a factor in coastal frontogenesis.

Using 57 coastal front cases, Bosart also presented a climatology of New England coastal fronts. As in the case study, the precipitation patterns revealed an axis of maximum precipitation just west of the preferred coastal front location, while the thermal patterns identified December as the month of greatest land-sea temperature contrast. This latter fact is consistent with the December maximum of coastal front occurrence.

Further investigation of the precipitation distribution associated with the coastal front was conducted by Marks and Austin(1979). Vertical sounding analyses of eight coastal front cases consistently identified a shallow region of convective instability at 600 mb with a neutral, well mixed layer above it. Analyses of radar observations indicated that precipitation was oriented in bands of convective cells which apparently originated from the advancing synoptic cyclone. The movement of these cells was consistent with the winds at the layer of convective instability. This pattern of convective instability associated with bands of convective cells is consistent with the cyclone model of Harrold(1973) as well as the case study results of Kreitzberg and Brown(1970).

The precipitation analyses of Mark's and Austin

reconfirmed Bosart's conclusion concerning higher precipitation values near the coastal front zone. Since the precipitation bands were a result of the synoptic cyclone, they hypothesized that coastal fronts produce a local intensification of the precipitation. Calculations of water vapor flux divergence revealed a flux convergence maximum over the frontal zone. Marks and Austin conclude that the mechanism for precipitation enhancement is the creation of low cloud, due to flux convergence, which allows for the accretion of water droplets onto the hydrometeors falling from the mesoscale bands.

Efforts to numerically model the coastal front phenomena were initiated by Ballentine(1980). He used a three-dimensional primitive equation model to investigate the effects of surface friction, latent heating, land-sea temperature contrast, synoptic sclale forcing and other physical properties upon coastal frontogenesis. The "basic model", which included all the physical effects, created a typical coastal front scenario. Low-level convergence developed near the coastline with strong vertical motions in the warm air east of the front.

Ballentine varied the model structure to identify the role of individual physical effects. The results indicated latent heat release and surface friction were not primary factors influencing coastal front circulation, however, land-sea temperature contrast and synoptic scale forcing

were identified as significant factors. Reducing the sea surface temperature 6 K decreased the backing of the winds over the land resulting in lessened convergence and vertical velocities near the coast. In the same fashion, removing the effects of an advancing 700 mb short wave significantly reduced the circulation within the coastal front zone.

A case of explosive cyclogenesis along a Carolina coastal front was analyzed by Bosart(1981). Three-dimensional analyses of the frontogenesis equation terms produced results remarkably similar to Sanders(1955). The confluence term dominated the frontogenetical effects. Vertical cross sections of winds normal to the front revealed strong lateral shear along the frontal boundary with significant vertical shear above the front. In addition, a zone of strong vertical motions was found along the warm boundary of the front. Bosart concluded that cyclogenesis initially resulted from strong low tropospheric warm air advection associated with the coastal front circulation. The front then acted as a steering mechanism for the cyclone until it came into phase with an intense short wave trough moving eastward from the Ohio Valley.

# 2. Data and Methodology

## 2.1 Surface and Upper Air Data

Data for this case study were obtained from the National Climatic Center. Hourly observations from civilian and military reporting stations, for the period 0000 GMT 21 - 0000 GMT 23 December 1983, were used to construct surface analyses. Wind and temperature observations from Coast Guard stations and offshore buoys were also used to better detect the development and onshore movement of the coastal front. The region of coverage included the Atlantic coastal states from New Jersey to Georgia as well as Tennesee, Kentucky and West Virginia.

Cross sections were constructed from radiosonde observations within the same region. Precipitation analyses were constructed from six-hourly data on airways observations and from hourly recording station networks.

## 2.2 Objective Analysis Scheme and Grid Contruction

Generating fields of kinematic variables as well as fields of gradients, fluxes and frontogenesis terms required the execution of numerous finite-difference calculations. To simplify the process, the Barnes(1964,1973) objective analysis scheme was used to create gridded fields of basic data. This particular scheme was selected for its simplicity, accuracy and cost effectiveness.

The Barnes scheme uses Gaussian weight functions to

generate the gridded values. Weights, $W_n$, are assigned to the original data, $f_n(x,y)$, based solely upon the distance, $d_n$, between the data and the grid point. Outside of a specified critical radius, $r_c$, a weight of zero is assigned to the data. This zero weight value is a local modification of the Barnes scheme which reduces computation time. A weight parameter, $k_o$, is externally choosen to determine the filter response function, $D_o$, which determines what percentage of an original wave's amplitude is retained in the interpolated field.

With one pass through the data, the filter response function can be shown to be

$$D_o = \exp((k_o * 2\pi/\lambda)^2) \qquad 2.1$$

where is a given wavelength. The values at the grid points are then calculated using Equation 2.2

$$g_o = f_n(x,y) * D_o \qquad 2.2$$

Barnes(1973) modified the original technique to decrease computation time. The revised version allows for a second "correction pass" through the data to receive the desired response for a given wavelength. This is acheived by reducing the weight parameter on the correction pass to a value of $k_1$ where

$$k_1 = \gamma * k_o$$

and where $\gamma$ is a parameter which forces the interpolated field to converge toward the observed field.

The computer program used for this analysis was

designed by Dewey Harms of this department as a part of the preliminary studies for the upcoming GALE project. As a part of his project, Harms(1985) conducted several tests on Barnes scheme results. Analyses of data created from a Midwest cyclone case indicated that a weight parameter of 250 $Km^2$ to 500 $Km^2$ yielded the minimum Root Mean Square Error values for most meteorological parameters. From this, Harms determined that the total response function(a measure of how closely the interpolated values match the observed values) for a wavelength of 190 Km(two times the average station spacing) was 0.936. A total response function value of 1 indicates an exact agreement.

Using this information and other guidelines from Harms, grid regions for surface and upper air analyses were developed. Harms suggested that grid point spacing should range from one half to one times the average spacing of data stations within the grid. The nearest neighbor concept suggested a surface station spacing over the region of concern was about 85 Km. The value of 60 Km was then selected for the surface grid spacing. Using the total response function calculated by Harms, the equations of the Barnes scheme were solved for the optimum weight parameter. A value of 400 $km^2$ was derived for the 60 Km spacing.

An upper-air grid was developed using the same procedures. A grid spacing of 150 Km was selected based upon a 280 Km station spacing. An upper air grid weight

parameter of 4600 $Km^2$ was derived, however, the resulting gridded data fields were clearly too "smooth". A series of tests using variuos weight parameters indicated that a value of 1000 $Km^2$ produced reasonable results.

Figure 2.1 shows the domain of the grids used in this experiment. The surface grid extends over the Atlantic to include the available buoy data and remove edge effects of the scheme away from the coast. Since effectiveness of the Barnes scheme is dependent upon the selected station spacing, "bogus" data were included at 1x1 degree locations over the ocean where the data void would adversely affect the results in the generated data fields. The effect of data paucity was a problem only in the southeast sector of the upper-air grid where one "bogus" sounding was added to the data. The "bogus" data were developed using available surface data from reporting stations and off-shore buoys, upper-air charts and radar film loops. In most cases, a linear interpolation was used to estimate parameter values.

## 2.3 Frontogenesis Calculations

Both the Eulerian and Lagrangian perspectives have distinct advantages when quantifying frontogenetic processes. The Eulerian method focuses upon processes which directly affect the intensity and motion following the front. Pettersen(1940) defined frontogenesis as the local derivative of the gradient of some conservative property S. Appendix A explains how equation 2.3 is derived from

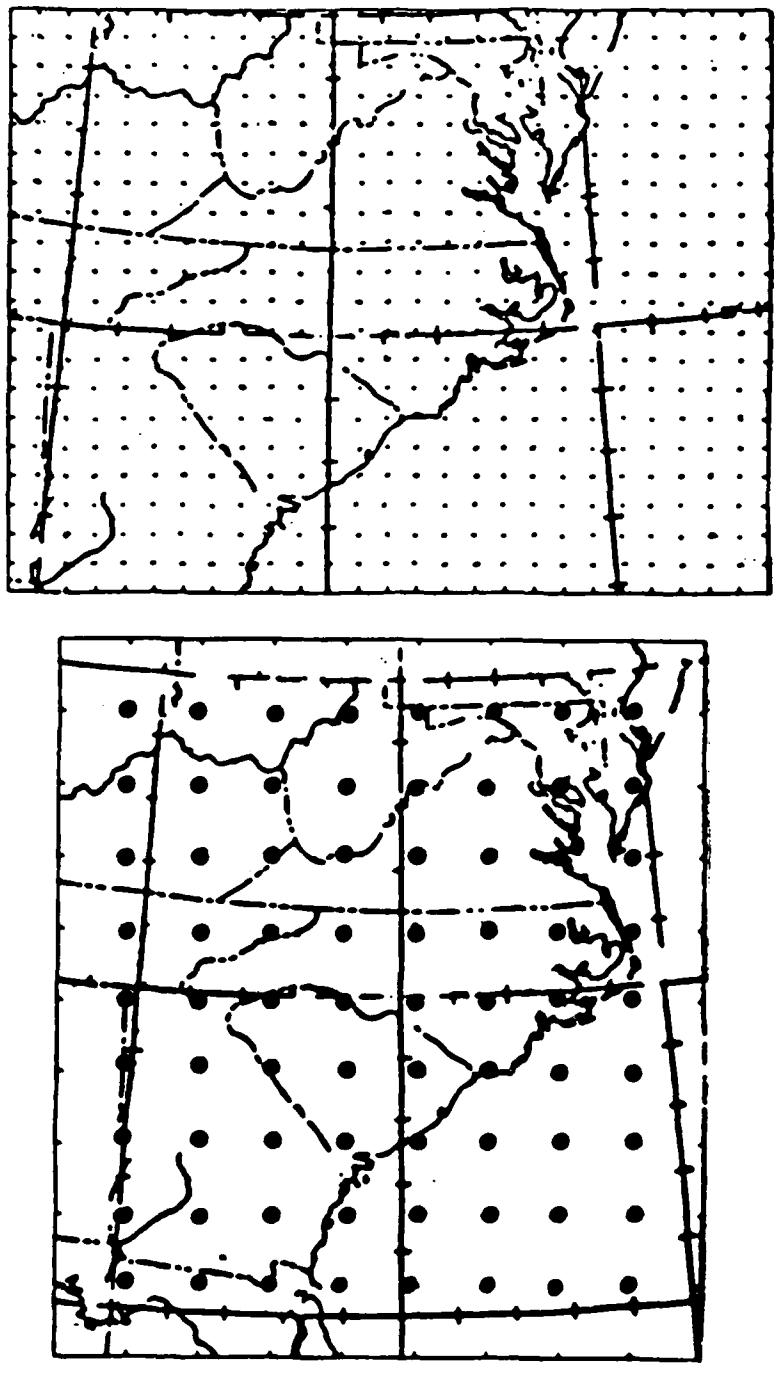

Figure 2.1. Illustration of grids used to analyze surface(top) and upper_air (bottom) data.

Petterssen's original formula, namely,

$$\partial/\partial t\ |\nabla S| = (1/|\nabla S|)*(\nabla S)\bullet[\nabla(-V_h\bullet\nabla S)+\nabla(w\bullet\nabla S)+\nabla(dS/dt)] \quad 2.3$$

$$\qquad\qquad\qquad\qquad\qquad\qquad\qquad\qquad\qquad\qquad A \qquad B \qquad C$$

The formula implies that frontogenesis is a function of the unit gradient vector dotted with the following: the gradient of horizontal S advection (term A), the gradient of vertical S advection (term B), and a differential diabatic term (term C). For our purposes, we will evaluate only term A and assume that terms B and C are negligible. This reduces equation 2.3 to

$$\partial/\partial t\ |\nabla S| = (1/|\nabla S|)*\nabla S\bullet\nabla(V_h\bullet\nabla S) \qquad 2.3.1$$

Figure 2.2 graphically interprets the frontogenesis processes of equation 2.3.1. The horizontal gradient vector is directed from low to high values of S(left to right). To the right of C, the horizontal gradient of S advection vector is directed downstream, while to the left of C, the horizontal gradient of S advection vector is directed upstream(low to high values). From equation 2.3, frontogenesis is expected to occur where the gradient of S advection is oriented in the same direction as the S gradient vector.

The Lagrangian viewpoint of frontogenesis focuses on the evolution of the temperature gradient following the motion of an air parcel. Defining frontogenesis as the total derivative of the gradient of the conservative property S, Newton(1954) derives equation 2.4 as the

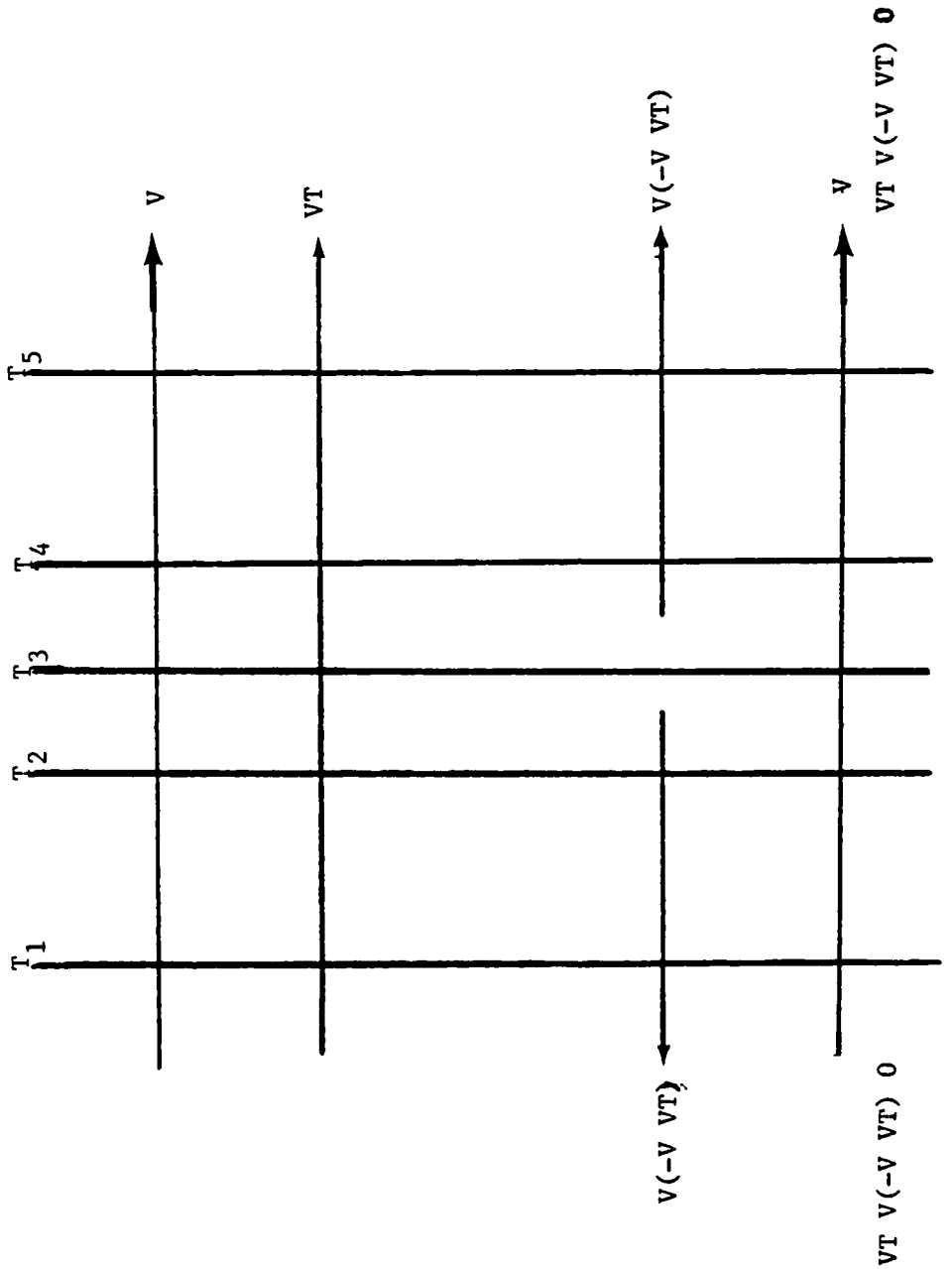


Figure 2.2. Illustration of effects of temperature and wind fields upon Eulerian frontogenesis. Wind flow is from left to right and $T_1 < T_5$.

horizontal components of the frontogenesis equation where the equation for $F_x$ is the similar to $F_y$.

$$F_y = d/dt(dS/dy) =$$

$$\partial/\partial y(dS/dt) - (\partial S/\partial x * \partial u/\partial y + \partial S/\partial y * \partial v/\partial y + \partial S/\partial z * \partial w/\partial y) \quad 2.4$$

A B C D

Term A represents the effect of differential diabatic heating or cooling and is difficult to graphically or numerically evalute. Terms B,C and D are illustrated in Figure 2.3. Term B represents the effects of horizontal shear, while term C represents the effect of lateral confluence. Term D illustrates the effect of the horizontal gradient of vertical velocity.

Both methods of assessing frontogenesis have distinct advantages. As previously stated, the Lagrangian method evaluates the frontogenetical effects of confluence, shear, and gradient of vertical velocity on a parcel of air as it flows through a given region. On the other hand, the Eulerian version reveals information concerning frontal movement. For example, if the magnitude of the gradient is increasing at the point where the gradient of S is already a maximum, it is clear that there is frontal intensification. Another advantage of the Eulerian version lies in the need to look only at the gradient of advection in relation to the temperature gradient. Both of these quantities are discernable from surface or upper-air charts.

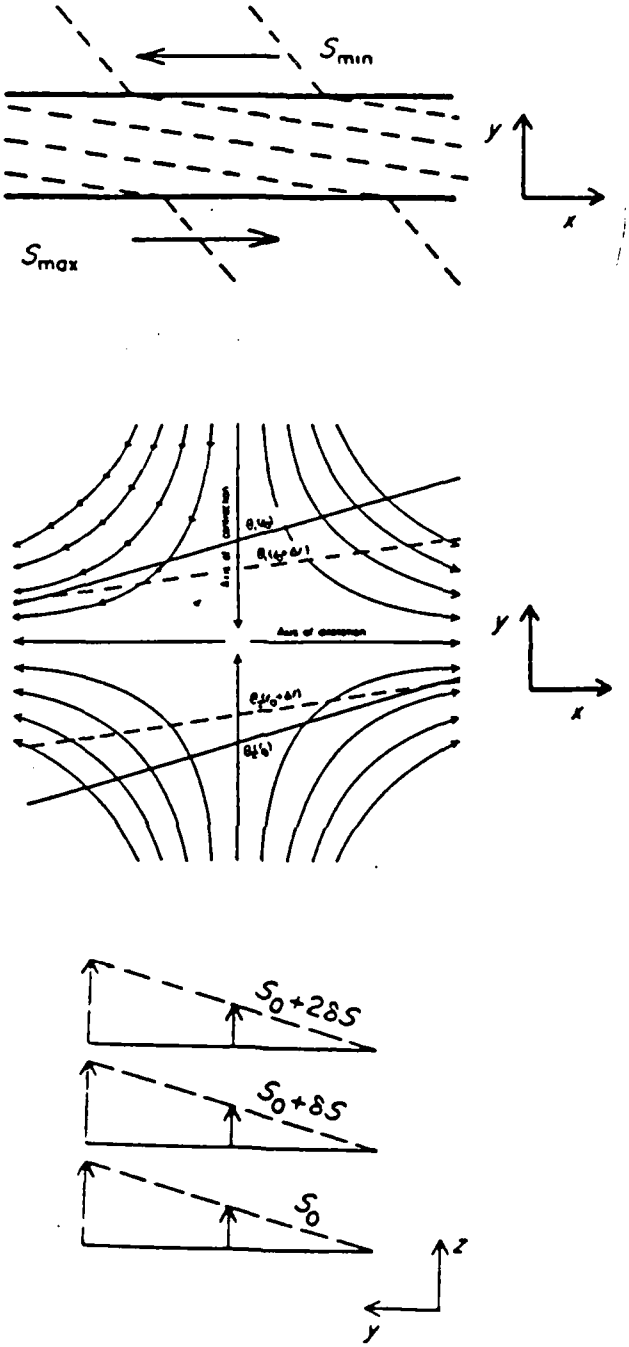


Figure 2.3. Illustration of effects of terms B(top), C(center) and D(bottom) in the Lagrangian frontogenesis equation(equation 2.4 in text).

## 2.4 Kinematic Calculations

Calculations of observed divergence, deformation and relative vorticity(about the vertical axis) are performed using the standard equations of Petterssen(1940). Vertical velocities are obtained using the kinematic method. The continuity equation in X,Y,P coordinates is expressed as:

$$\partial u/\partial x + \partial v/\partial y + \partial w/\partial p = 0 \qquad 2.5$$

Integration in the vertical yields:

$$(\partial w/\partial p)dp = \nabla\bullet\int V_h \, dp \qquad 2.6$$

In finite-difference form, the vertical velocity at a pressure level is obtained from equation 2.7

$$w_u = w_l - \nabla\bullet\bar{V}_h * (p_u - p_l) \qquad 2.7$$

where $w_u$ is the vertical velocity at the upper pressure level

$w_l$ is the vertical velocity at the lower layer

$p_u$ is the upper pressure level

$p_l$ is the lower pressure level

$\nabla\bullet\bar{V}_h$ is the horizontal divergence of the layer mean wind

The layers used to calculate layer mean divergences were the surface to 975 mb layer and successive 25 mb layers up to 800 mb and succesive 50 mb layers up to 500 mb.

# 3. Analysis of the Coastal Front

## 3.1 Synoptic Overview

Figure 3.1 illustrates the 12-hourly surface and 500 mb charts for the period 1200 GMT 21 December through 0000 GMT 23 December 1983. During this period the ridge over the eastern U.S. progresses eastward while an outbreak of arctic air moves southward from the Northern Plains States. An upper-air cutoff-low develops and advances eastward over the northern Great Lakes region.

The surface pattern shows a dome of high pressure centered over New England and eastern Canada. As the major axis of the ridge progresses eastward, an anticyclonic bulge develops east of the Appalachians. By 0000 GMT 22 December, a trough develops along the Mid-Atlantic coastal region in association with a well defined mesoscale frontal zone. By 1200 GMT, the trough progresses inland and a weak low center evolves near the North Carolina-Virginia border. At 0000 GMT 23 December, the synoptic scale cold front associated with the outbreak of cold air in the Midwest, progresses into the western Carolinas and begins to overwhelm the mesoscale features associated with the coastal front.

## 3.2 Mesoscale Analysis

Figure 3.2 offers a detailed mesoscale perspective of coastal front evolution. Ship data was rarely available, however, data from the offshore buoys are significant in

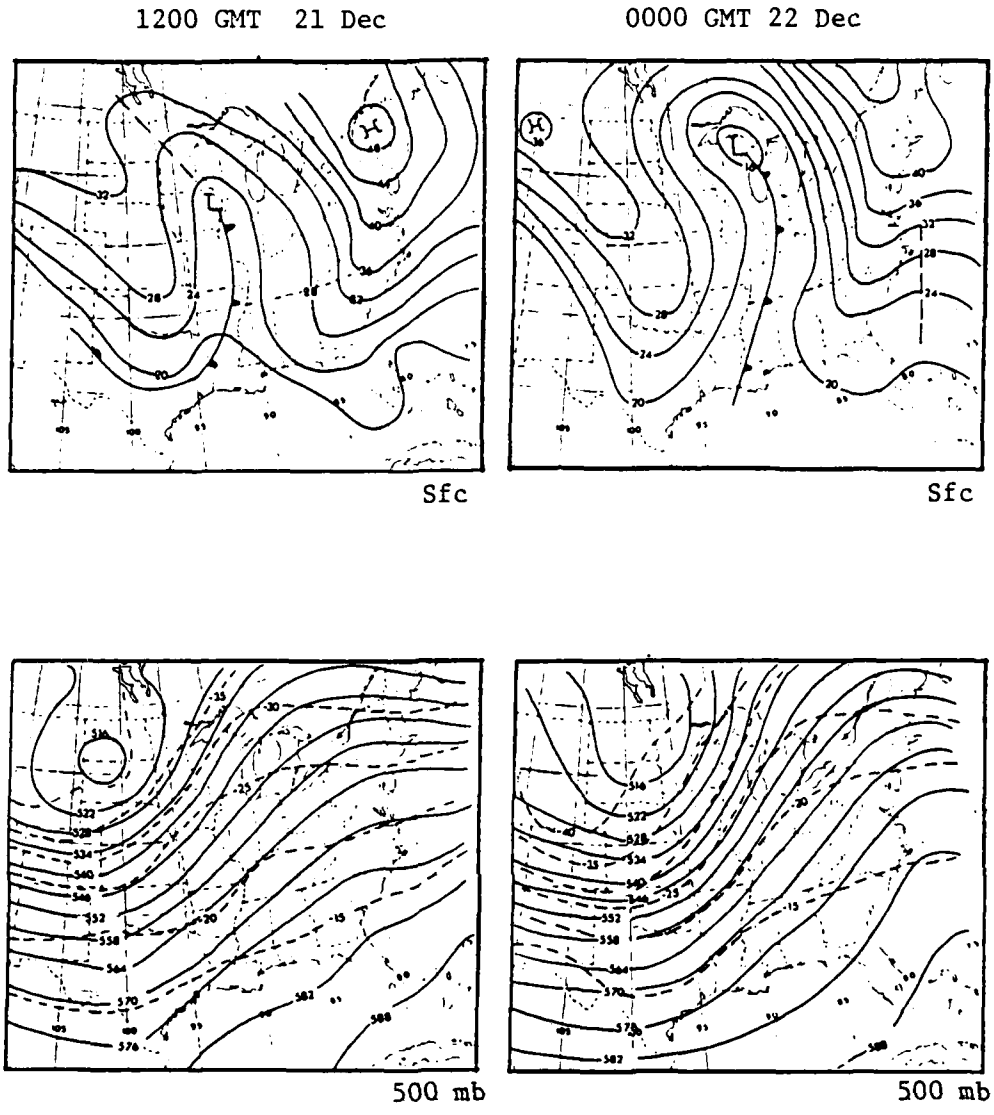


Figure 3.1. Surface and 500 mb maps for 21-23 December 1983. Standard plotting analysis is used. Solid lines represent 500 mb heights, in decameters, and surface pressures, in millibars in excess of 1000. 500 mb isotherms are in $^{o}C$. National Weather Service products were used to develop the analyses.

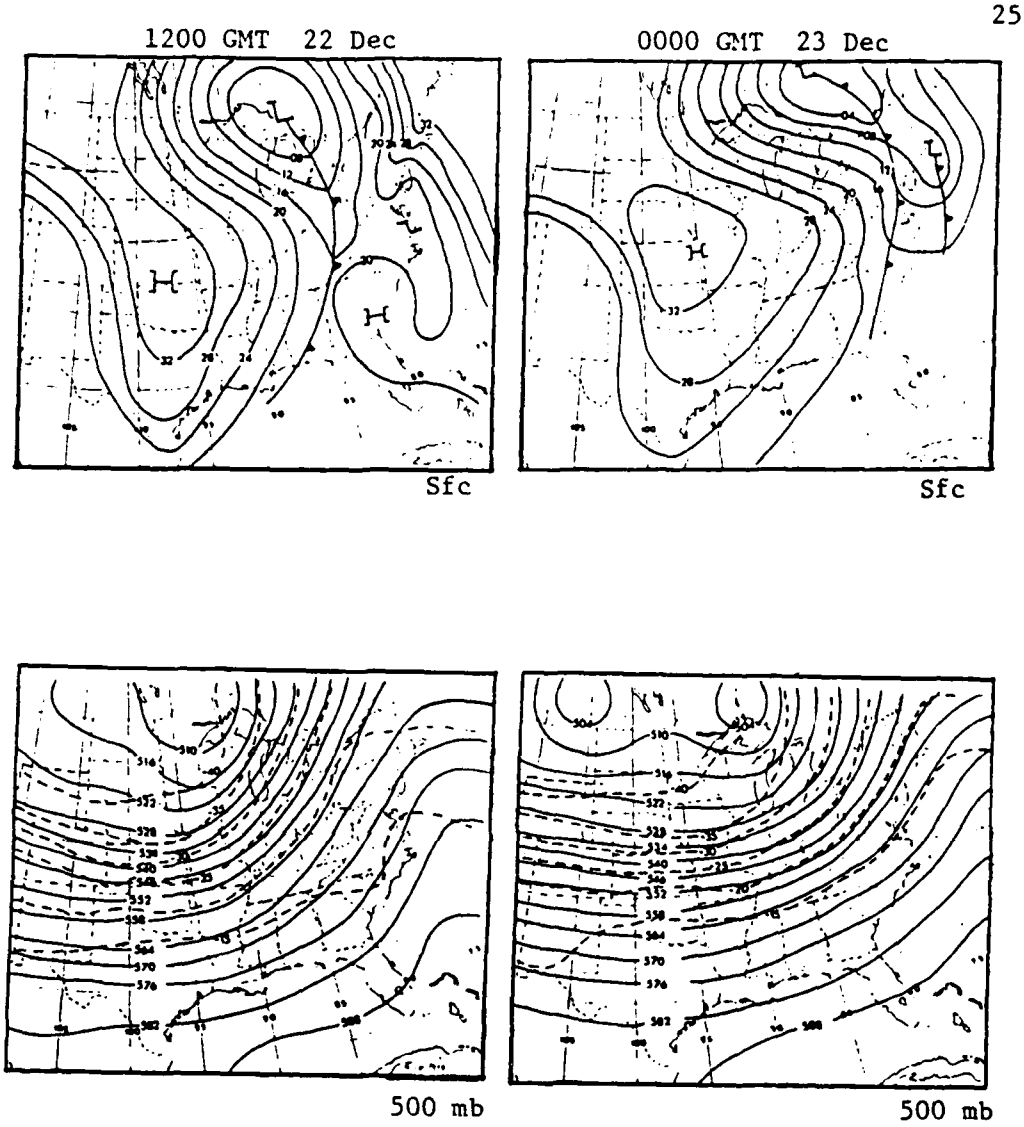


Figure 3.1. (continued)

identifying and tracking the coastal front evolution. At 1800 GMT 21 December the pressure pattern reveals the developing trough over the Atlantic and the increasingly ageostrophic flow over the land. In particular, winds near the coast are nearly geostrophic while at the axis of the anticyclonic bulge the winds are nearly perpendicular to the isobaric pattern and parallel to the isotherm distribution. Since the flow inland results in weak cold air advection while the coastal flow favors significant warm air advection, the net effect of continued ageostrophy would enhance frontogenesis near the coast.

At 0000 GMT 22 December the thermal pattern indicates an increase in the isotherm packing along the coastal region of the Carolinas and Virginia. Further evidence of offshore trough development is offered as the buoy data reveals a shift to southeasterly winds. Cape Hatteras, NC(HAT) also indicates a gradual shift from a northeasterly to a southeasterly flow with an increase in the sustained and gust wind speeds. The anticyclonic bulge and associated ageostrophic flow remains firmly entrenched east of the mountains maintaining slight cold air advection down the axis of the ridge.

The 0600 GMT 22 December analysis affords the most interesting view of the coastal front. In particular, winds all along the coast from Charleston, SC(CHS) to Atlantic City, NJ(ACY) have shifted to the southeast with a

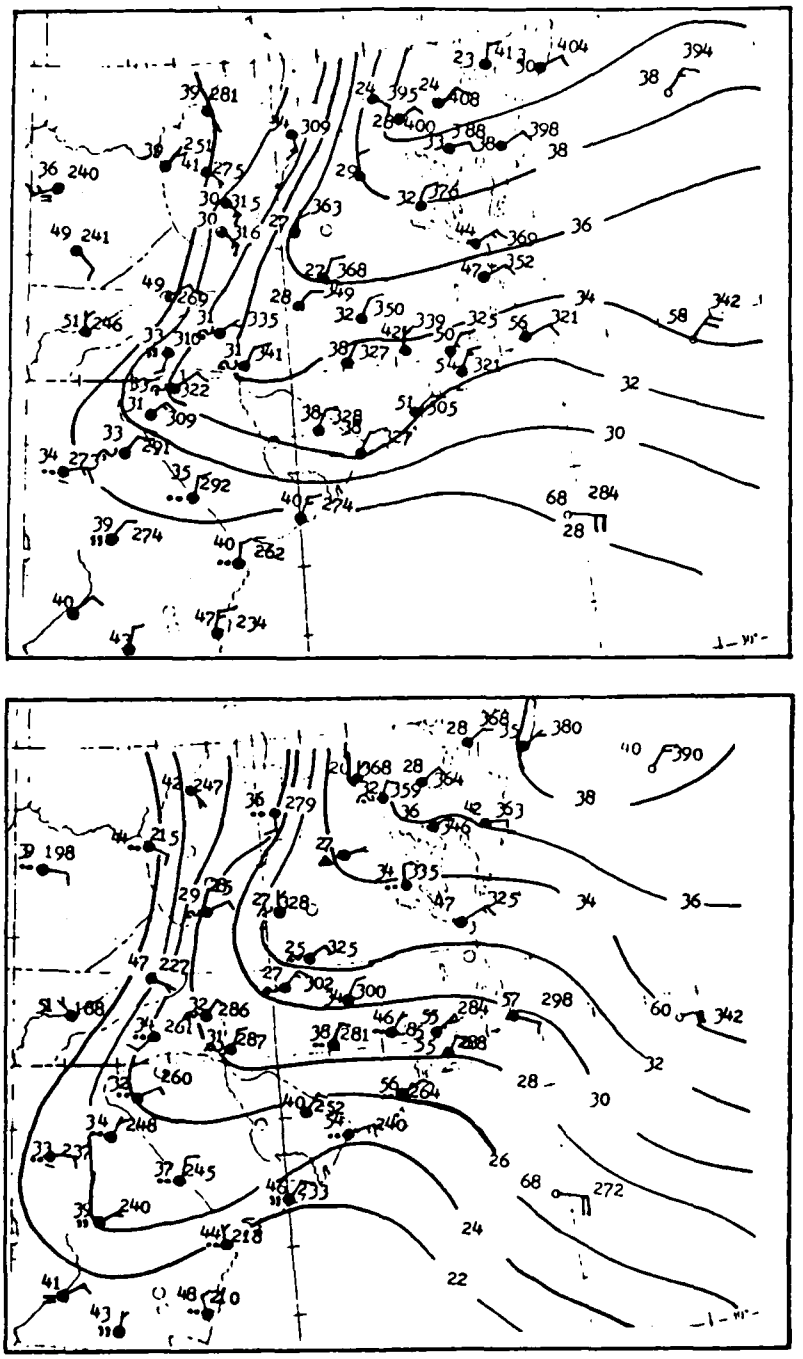

Figure 3.2. Mesoscale surface analyses for 1800(a) 21 December 1983, 0000(b), 0600(c), 1200(d) and 1800(e) 22 December 1983. Solid lines represent pressure. Temperatures are in °F, winds are in m/s(full(half) barb=5(2.5)m/s) and pressures are in millibars in excess of 1000.

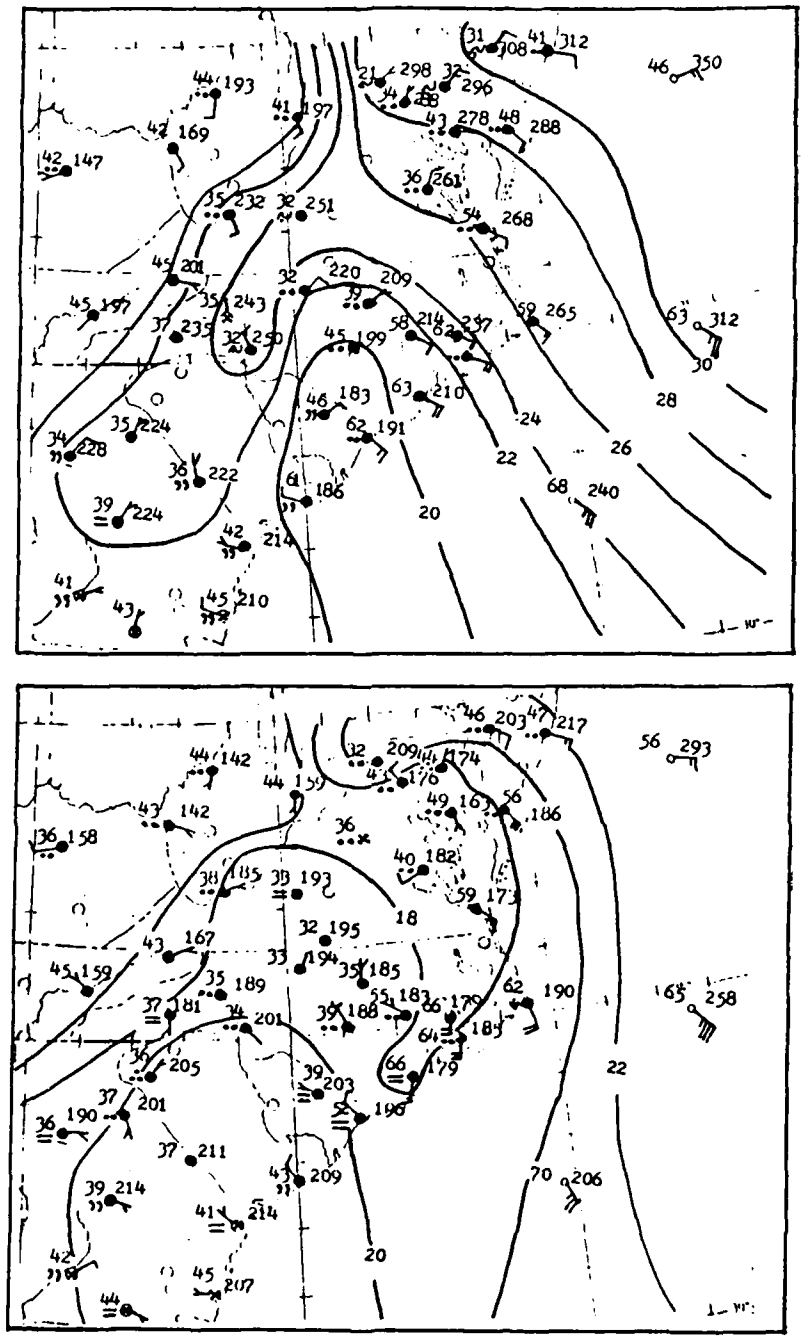

Figure 3.2. (continued)

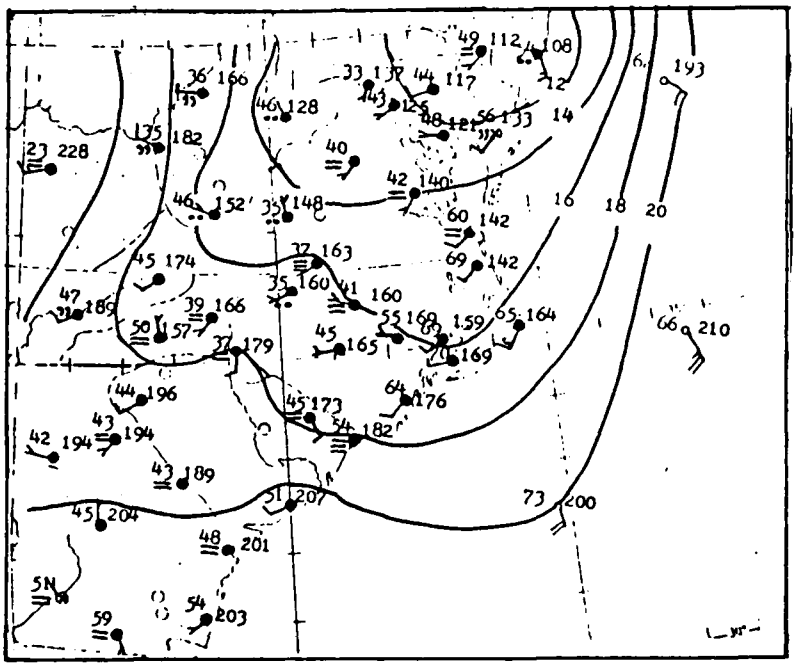


Figure 3.2. (continued)

significant increase in sustained and gust wind speeds. The associated trough shifts inland significantly and appears to sever the anticyclonic bulge over central North Carolina and western Virginia. The total wind field indicates a strong convergence zone along coastal South Carolina and just inland along North Carolina and Virginia. Temperatures along the Carolina coasts are increasing at modest rates, however, the startling temperature contrast lies between CHS and the Naval Air Station at Beaufort, SC A temperature of 289K (291K the previous hour) at CHS compared with a temperature of 280K at Beaufort converts to a temperature gradient of approximately 1K/10Km. Considering that this gradient is oriented somewhat along the frontal zone, the true cross front gradient is probably much greater.

At 1200 GMT 22 December, the anticyclonic bulge which dominated the inland flow early in the period is non-existent. The coastal front moves offshore along South Carolina while strong southeasterly winds along the coast converge with northwesterly winds inland to increase the temperature gradient along the eastern third of North Carolina. By 1800 GMT 22 December, the strong temperature contrast still exists across Virginia and North Carolina, however, the characteristic convergent flow associated with the front no longer exists. A weak cyclone center located along the Carolina coast at 1200 GMT progresses northeastward and deepens through the 1800 GMT 22 December

time period. The circulation associated with this cyclone results in a westerly flow over most of the region. The net result is a gradual diffusion of the temperature gradient associated with the coastal front.

Figure 3.3 illustrates the temperature and wind profiles for selected stations for the time period 1800 GMT 21 December to 1800 GMT 22 December. Analysis of these profiles reveals some interesting characteristics of the coastal front. At CHS, Pope AFB, NC(POB) and Richmond, VA(RIC) a sharp rise in temperature over a one to three hour period is preceded by a shift to southeasterly winds, however, at other coastal stations like Langley AFB, VA and HAT and New Bern, NC(EWN) the shift to southeasterly winds results in minor, if not, negligible temperature rises. The fact that inland stations experience significant temperature increases with the shift to southeast winds while some coastal stations experience minimal temperature increases suggests that the coastal frontogenesis process is not always limited to the immediate coastal region. Previous description of the coastal front link sensible heating of the surface layer over the ocean with land-sea differential friction effects to create conditions favorable for frontogenesis at the coastline. If coastal frontogenesis always occurs in this manner, we should expect the temperature profile at HAT to imitate the profile at CHS. Instead, the profile of POB seems to resemble the CHS

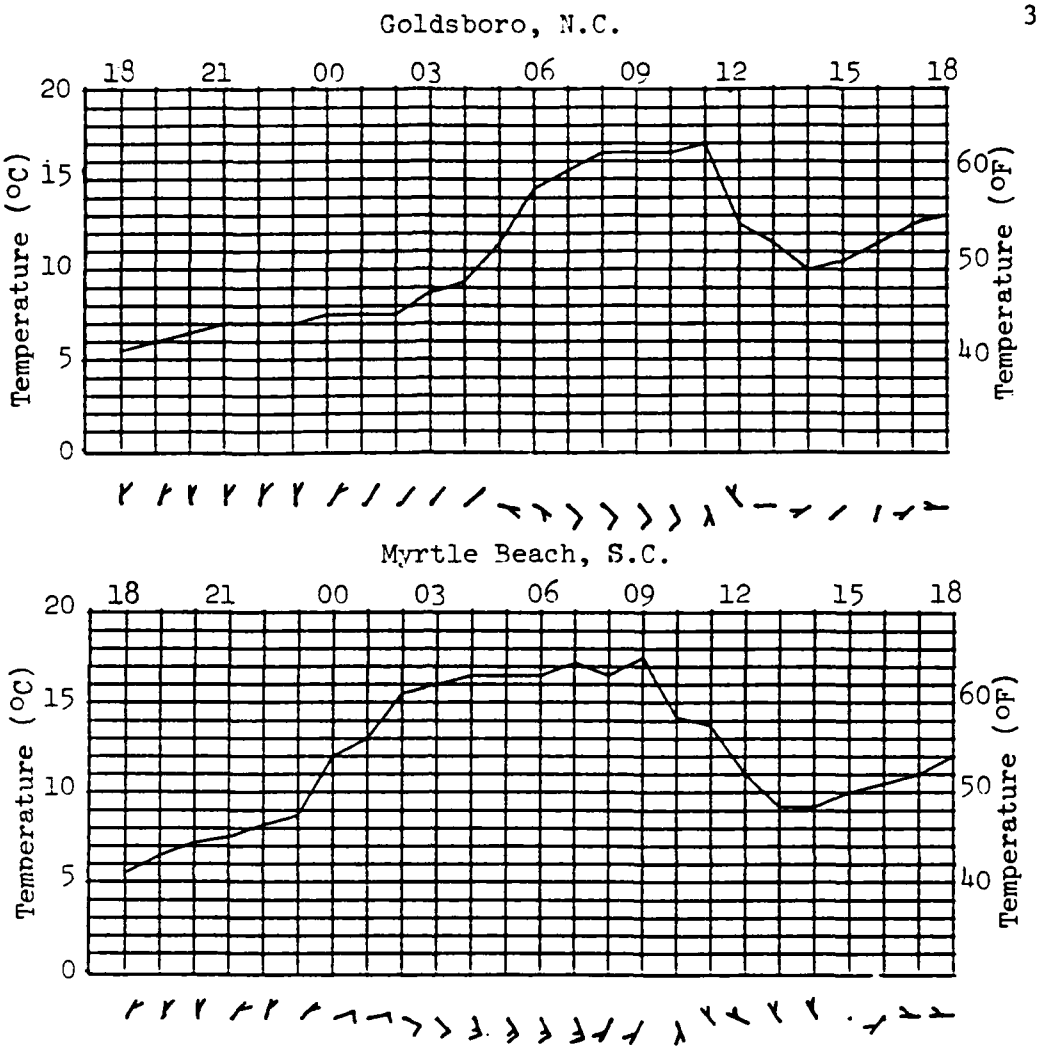


Figure 3.3. Temperature and wind profiles for the period 1800 GMT 21 December to 1800 GMT 22 December 1983 for selected stations within the coastal front zone. Wind designations are as in Figure 3.2.

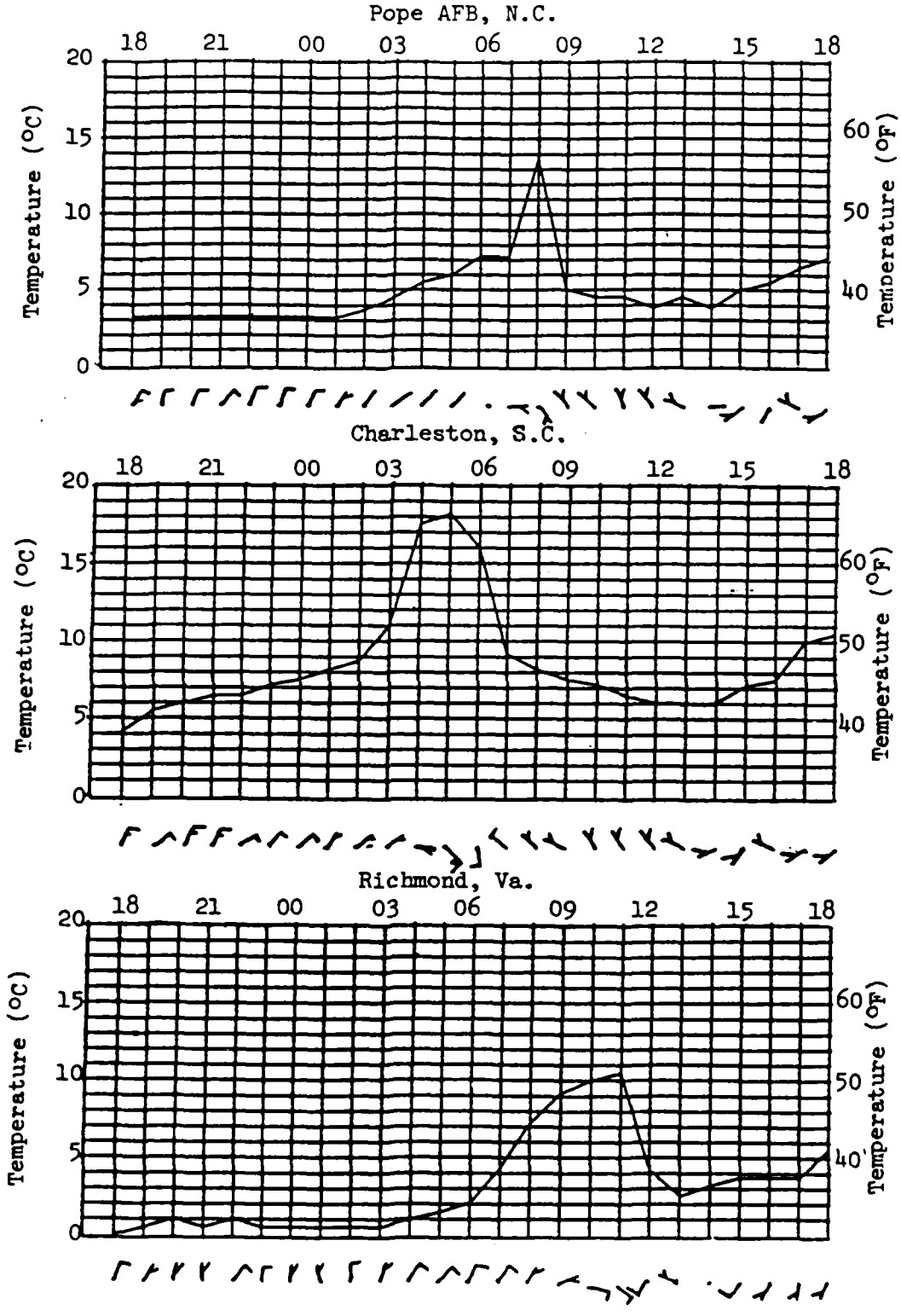


Fig. 3.3. Continued

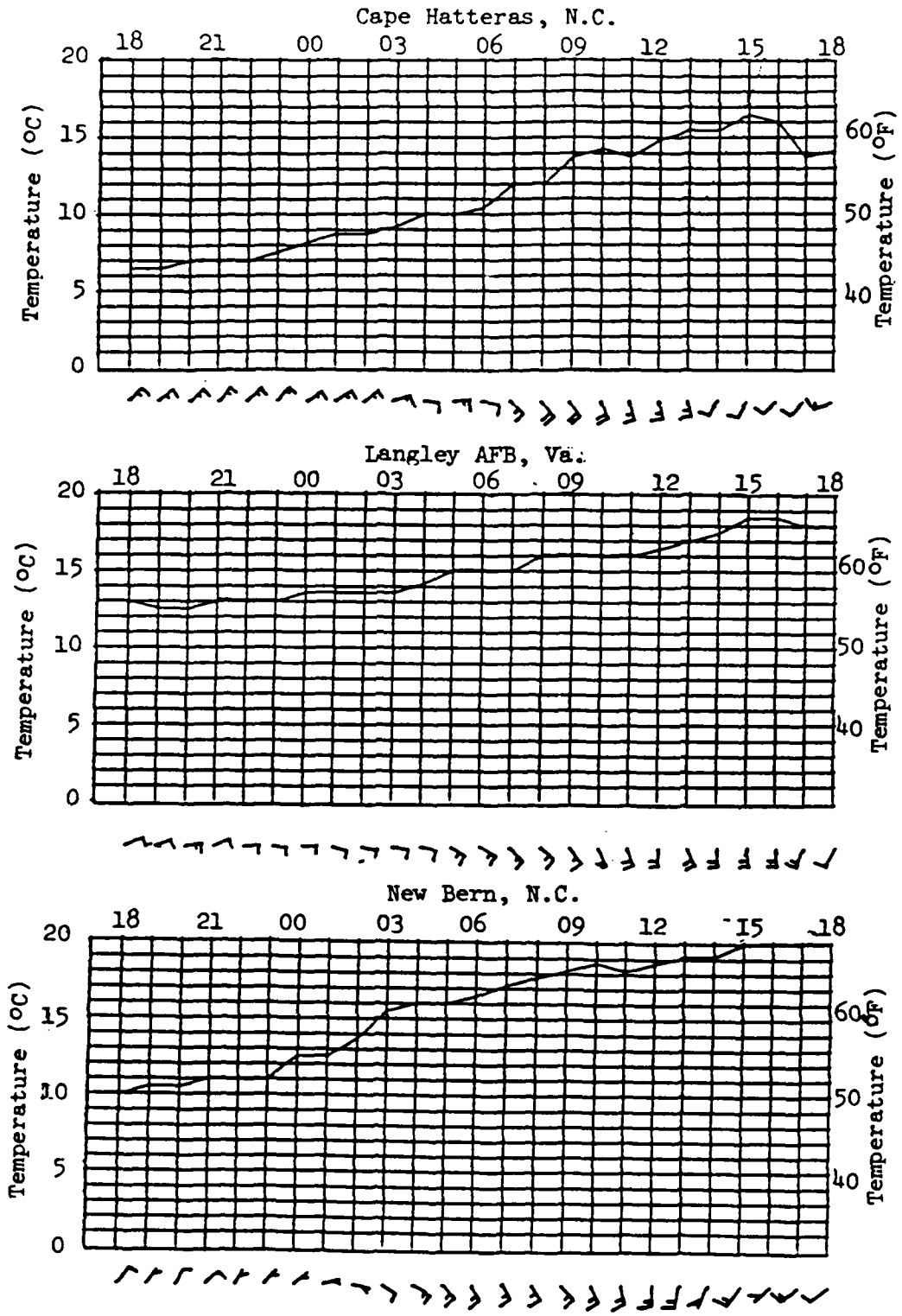


Fig. 3.3. Continued

pattern the closest. At CHS, POB and even RIC the equally sharp temperature variations seem to indicate that the front is approximately a steady state phenomena at the time it passes these locations(assuming a constant rate of movement). In contrast, at Seymour Johnson AFB, NC(GSB) and Myrtle Beach, SC(CRE) moderate temperature increases associated with the southeasterly winds are followed by smaller temperature increases over the next three to four hours. At these same stations temperature decreases, in association with a retreating coastal front, are much more acute. These observations suggest that atmospheric processes favored frontogenesis along the coastline east of CHS, however, it appears that frontogenesis was occurring over the land in eastern North Carolina.

3.3 Kinematic Analyses

The analysis of kinematic variables is useful for relating the characteristics of the wind field to the generation and maintenance of a frontal zone. Figures 3.4 through 3.7 display fields of divergence, relative vorticity, deformation and sea level geostrophic deformation at six-hourly time periods from 0000 GMT to 1800 GMT 22 December 1983. Grid spacing for all finite difference calculations was 60 Km. Values over the open ocean must be considered suspect since they are mostly generated from the "bogus" data mentioned earlier.

At 0000 GMT the divergence and relative vorticity

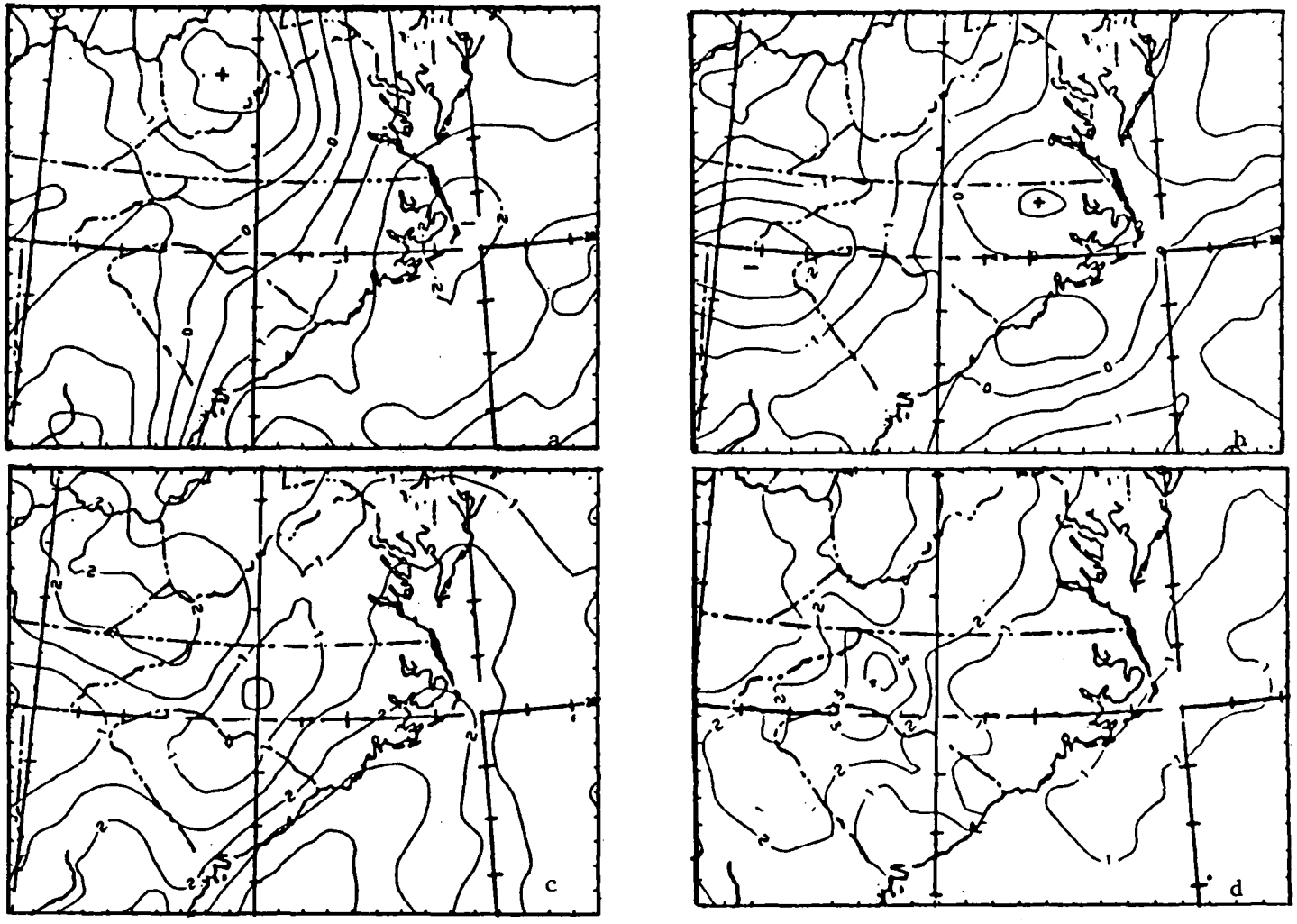


Figure 3.4 Divergence(a), relative vorticity(b), observed deformation(c) and geostrophic deformation(d) for 0000 GMT 22 December. Units are $10^{-5}$ $s^{-1}$. Contour intervals are every .5 units for (a), (b) and (c) and every 1 unit for (d).

patterns are consistent with previous coastal front analyses. A broad region of divergence and negative relative vorticity associated with the anticyclonic bulge, extends along the Appalachian chain. The positive vorticity region is negligible at this time, however, a broad region of convergence extends along the coast. The convergence maximum over HAT is consistent with the shift to southeasterly winds at that location. The observed deformation maximum parallels the coast while the geostrophic deformation is located well inland. These results are quite similar to the findings of Bosart(1975). The inland maximum of geostrophic deformation aligns well with the strong anticyclonic curvature of the high pressure bulge.

By 0600 GMT (Fig. 3.5) the relative vorticity and convergence fields shift significantly westward as does the observed deformation field. These patterns correspond well with the surface trough which moved inland at this time. Strong southerly winds at the coastline and notherly wind over the interior translate to strong convergence values along the coastal region. Also, the vorticity maximum coincides with the nearly closed cyclonic circulation between Myrtle Beach and CHS. Considering the magnitudinal increases of these fields and that the axis of dilatation associated with the observed deformation field is oriented parallel to the coast and the isotherm pattern, it is

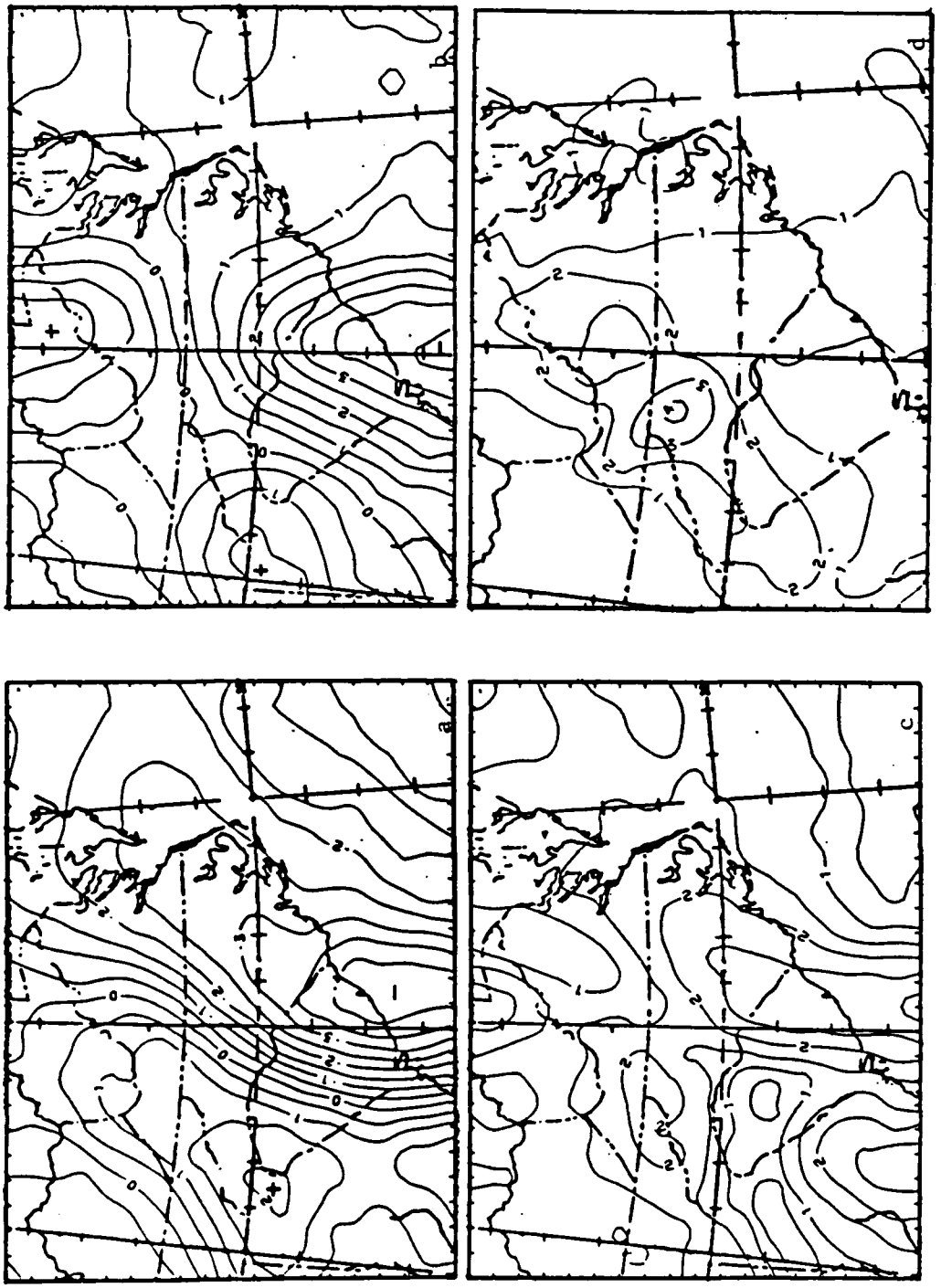


Figure 3.5. Same as Figure 3.4 except for 0600 GMT 22 December 1983.

reasonable to expect an increase of the temperature gradient over the coastal region.

The 1200 GMT relative vorticity and divergence fields (Fig. 3.6) undergo a significant change. The major axes of the positive relative vorticity and convergence shift eastward and the convergence maximum slides northwards to the Chesapeake Bay. The wind pattern confirms the shift of the convergence maximum as northwest winds over northeast Virginia and strong southeasterly winds over eastern Maryland indicate a strong convergent flow. The geostrophic deformation maximum previously located along the Appalachians has diminished significantly. The diminishing geostrophic deformation pattern correlates well with the dissipation of the anticyclonic bulge. The observed deformation field begins to deteriorate at this time also. These particular conditions provide additional evidence that the coastal front has probably reached its maximum intensity and has made its farthest inland penetration.

At 1800 GMT (Fig. 3.7) the vorticity, observed deformation and divergence patterns confirm that the Carolina coastal plains region is no longer favorable for frontogenesis. The positive vorticity maximum over the ocean is especially suspect considering that the cyclonic flow is located farther north. The convergence maximum over West Virginia is undoubtedly in conjunction with the advancing synoptic scale cold front.

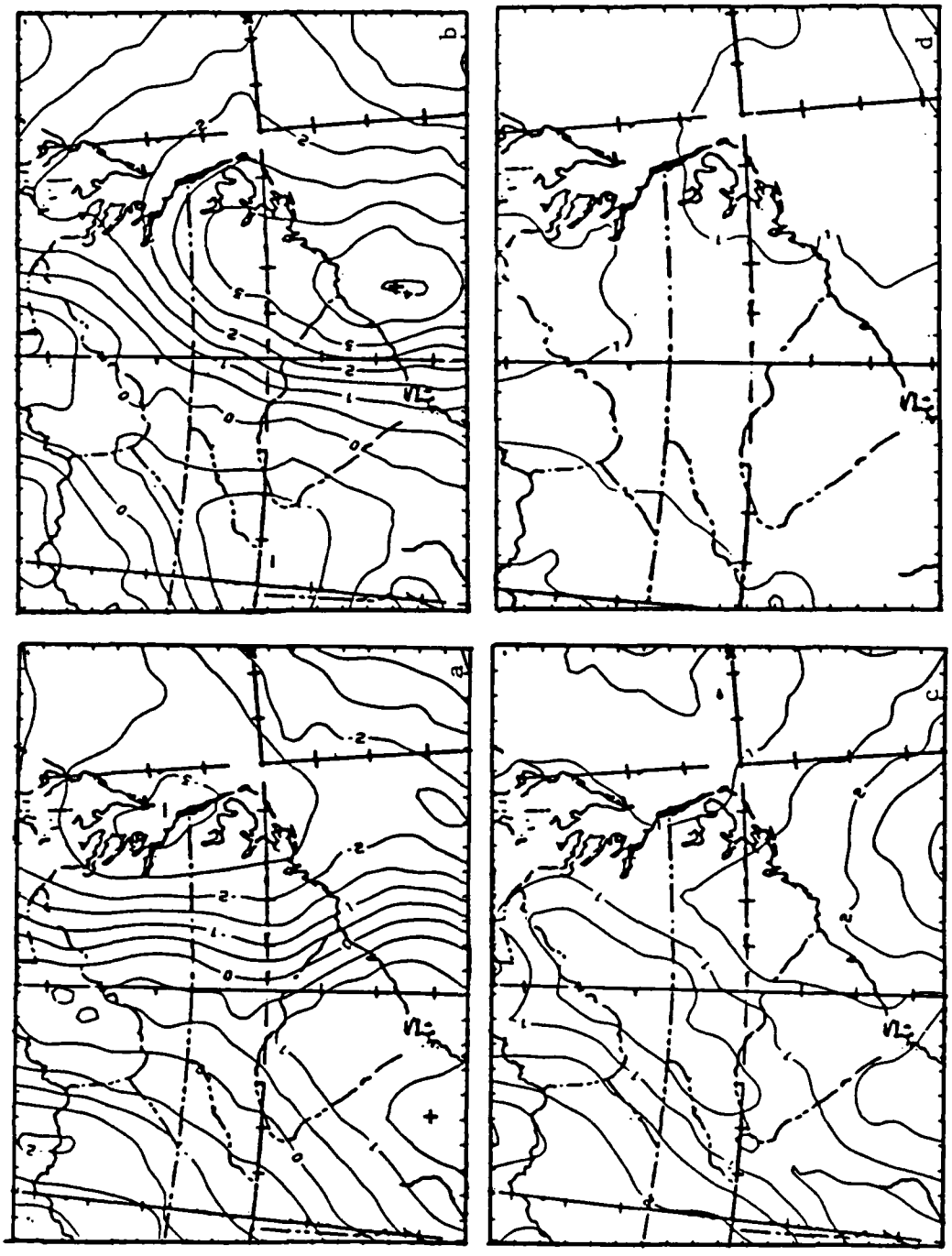


Figure 3.6. Same as Figure 3.4 except for 1200 GMT 22 December 1983.

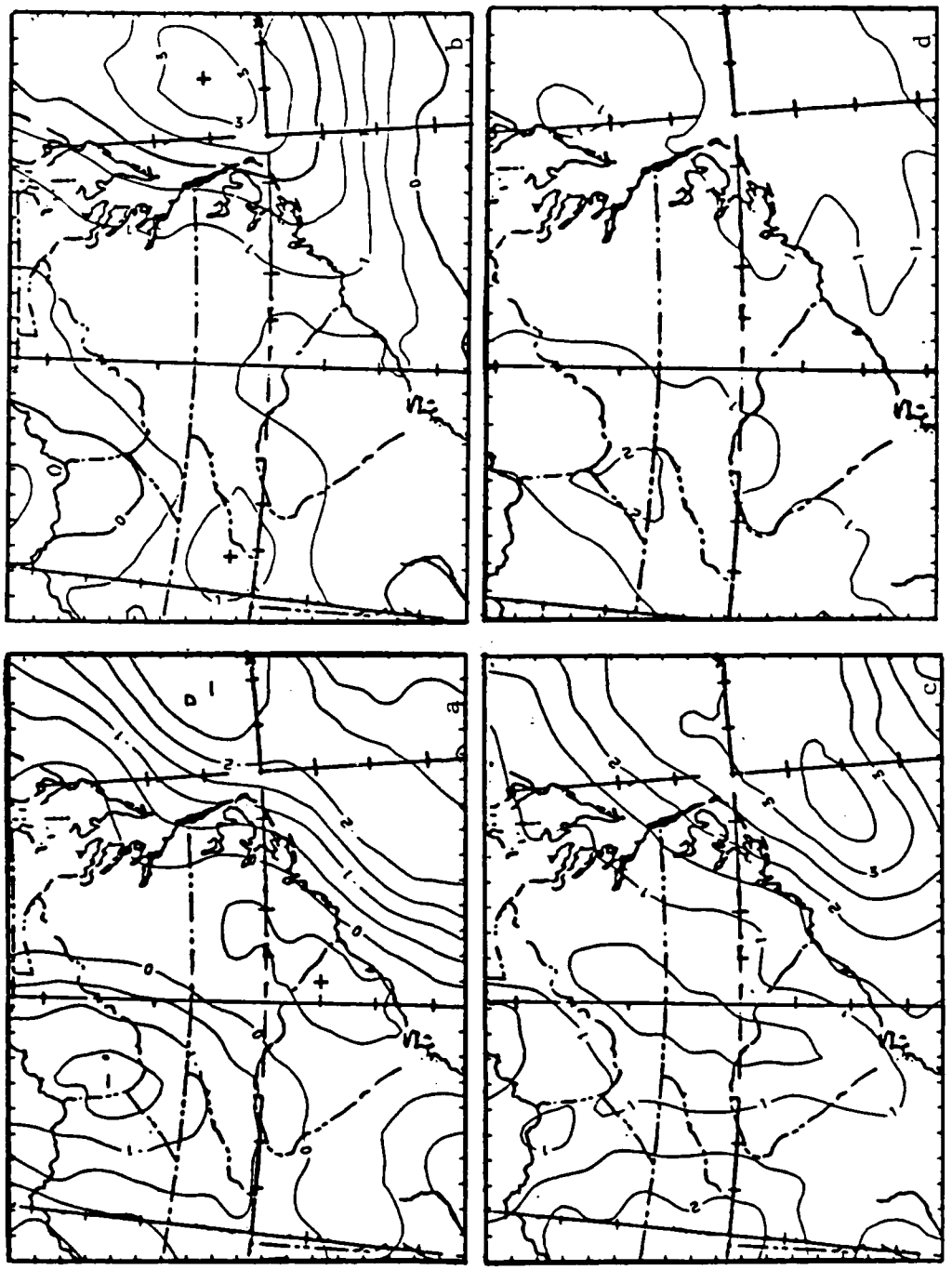


Figure 3.7. Same as Figure 3.4 except for 1800 GMT 22 December 1983.

## 3.4 Surface Frontogenesis Calculations

By definition, a frontal zone is a region of relatively strong temperature gradient. Changes in the temperature gradient pattern should reflect changes in frontal intensity and location. Fig. 3.8 illustrates the potential temperature gradient field at three-hourly intervals from 0000 GMT to 1500 GMT 22 December 1983. The patterns display a region of strong temperature gradient along the coastline from South Carolina to Maryland. Although the temperature gradient maximum shift slightly westward between 0000 GMT and 0600 GMT and then retreats eastward throughout the remaining periods, no significant change in the temperature gradient magnitude is displayed. These results give little indication of significant frontogenesis along the coastal region.

### 3.4.1 Lagrangian Frontogenetical Analysis

To assess the surface frontogenetical features from a Lagrangian perspective, Equation 2.4 in Section 2.2 is evaluated. Centered differencing is used to evaluate all derivatives. The diabatic term and the "tilting" term are not evaluated.

Figure 3.9 displays the total frontogenetical field at three-hourly intervals from 0000 GMT to 1500 GMT 22 December. In general, the shear term magnitudes were much less than that of the confluence term, therefore the frontogenetical fields for the individual terms are omitted

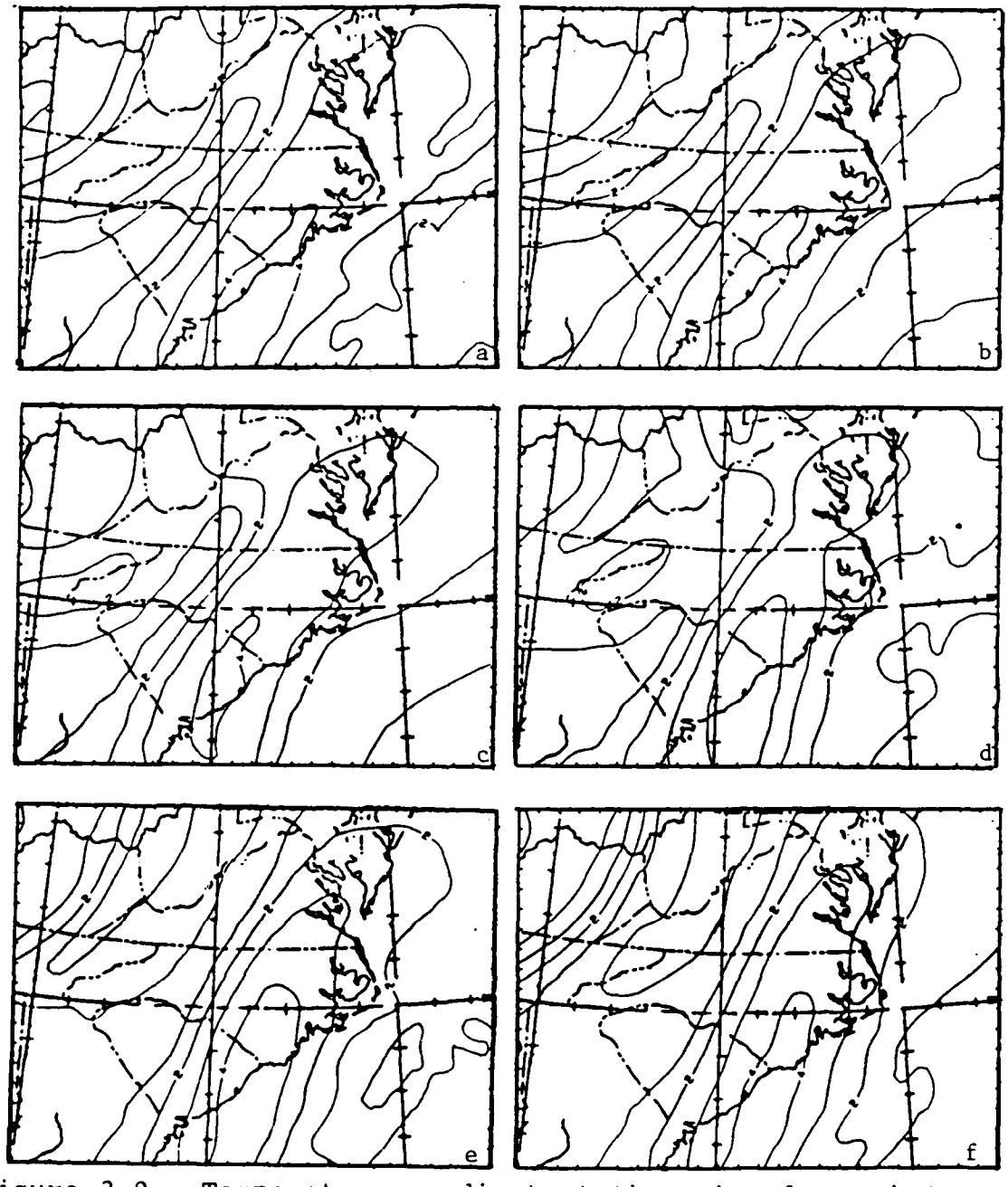


Figure 3.8. Temperature gradient at three-hourly periods from 0000 to 1500(a-f) GMT 22 December 1983. Units are $10^{-6}$ K $m^{-1}$. Contour interval is every 1 unit.

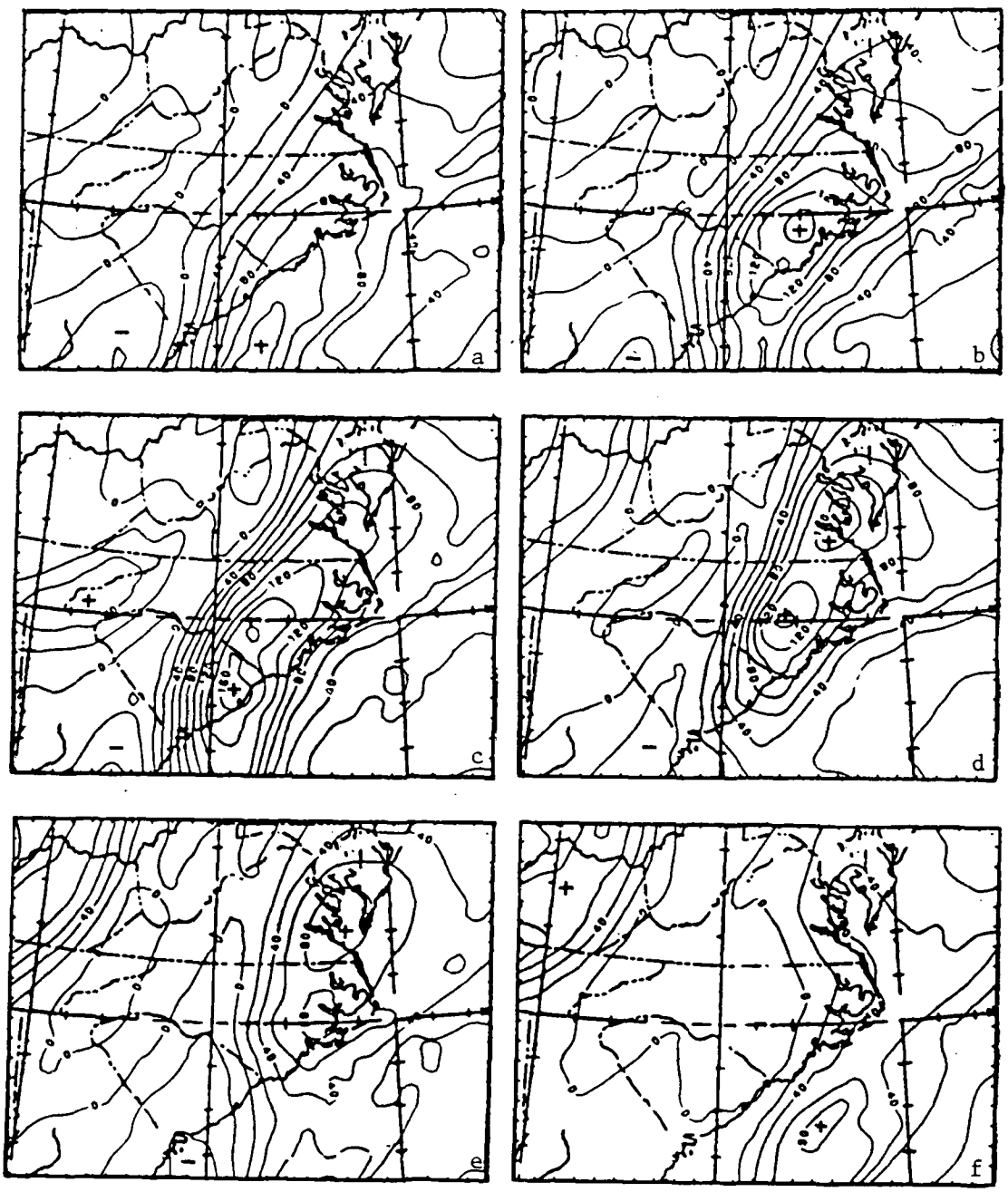


Figure 3.9. Lagrangian(total) frontogenesis for three-hourly periods from 0000 to 1500(a-f) GMT 22 December 1983. Units are $10^{-11}$ K $m^{-1}$ $s^{-1}$. Positive values indicate frontogenesis. Contour intervals are every 20 units.

from the diagrams. Units of frontogenesis can be multiplied by $10^8$ to yield units of approximately K (10 Km) $(3Hr)^{-1}$. At 0000 GMT, a broad region of frontogenesis parallels the entire coastal region with the maximum values along the coast of the Carolinas. At 0300 GMT and 0600 GMT the frontogenetical field indicates a significant increase in the temperature gradient tendency over eastern South Carolina and southeastern North Carolina. These sharp increases reflect the broad onshore flow in this region and are consistent with the increasing convergence values along the coastal regions.

By 0900 GMT the frontogenesis field signals a rapidly increasing temperature gradient tendency over eastern North Carolina while along the South Carolina coast the frontogenesis values have decreased. This pattern is consistent with the eastward movement of the coastal front away from CHS and the maximum inland penetration of the front in North Carolina. At 1200 GMT the frontogenesis maximum shifts further eastward and decreases in magnitude giving indications that the coastal front is retreating. At this time, the winds over the interior are predominantly from the north while the coastal winds are shifting to the south. The horizontal shear associated with this flow pattern is consistent with maintaining an existing frontal zone, however, it is not as conducive to increasing frontal intensity. This may account for the decrease in the overall

frontogenesis magnitudes and the fact that the shear and confluence terms are now about equal in magnitude. The frontogenesis field loses further definition at 1500 GMT as a southwesterly flow begins to dominate the entire region.

3.4.2 Eulerian Frontogenetical Analysis

The Eulerian frontogenesis calculations for this analysis are based upon Equation 2.3 in Section 2.2. The frontogenesis values are a function of the unit gradient vector dotted with the gradient of advection. In essence, the results of these calculations represent the effects of the thermal advection field, derived by the Barnes analysed data, upon the local change of the temperature gradient. Again, the values can be multiplied by $10^8$ to obtain units of approximately K (10Km) $(3Hr)^{-1}$.

Figure 3.10 shows the Eulerian frontogenesis patterns at three-hourly time periods from 0000 GMT to 1500 GMT 22 December. At 0000 GMT and 0300 GMT a weak region of frontogenesis over the coastal region of South Carolina is co-located with the temperature gradient maximum, in Fig. 3.8, along the coastal region of the Carolinas. As described earlier this pattern suggests an increase in the frontal zone temperature gradient without significant frontal movement over South Carolina and slight westward movement over North Carolina. The configuration of the frontogenesis field changes at 0600 GMT as the maximum shifts westward. Considering the previous location of the

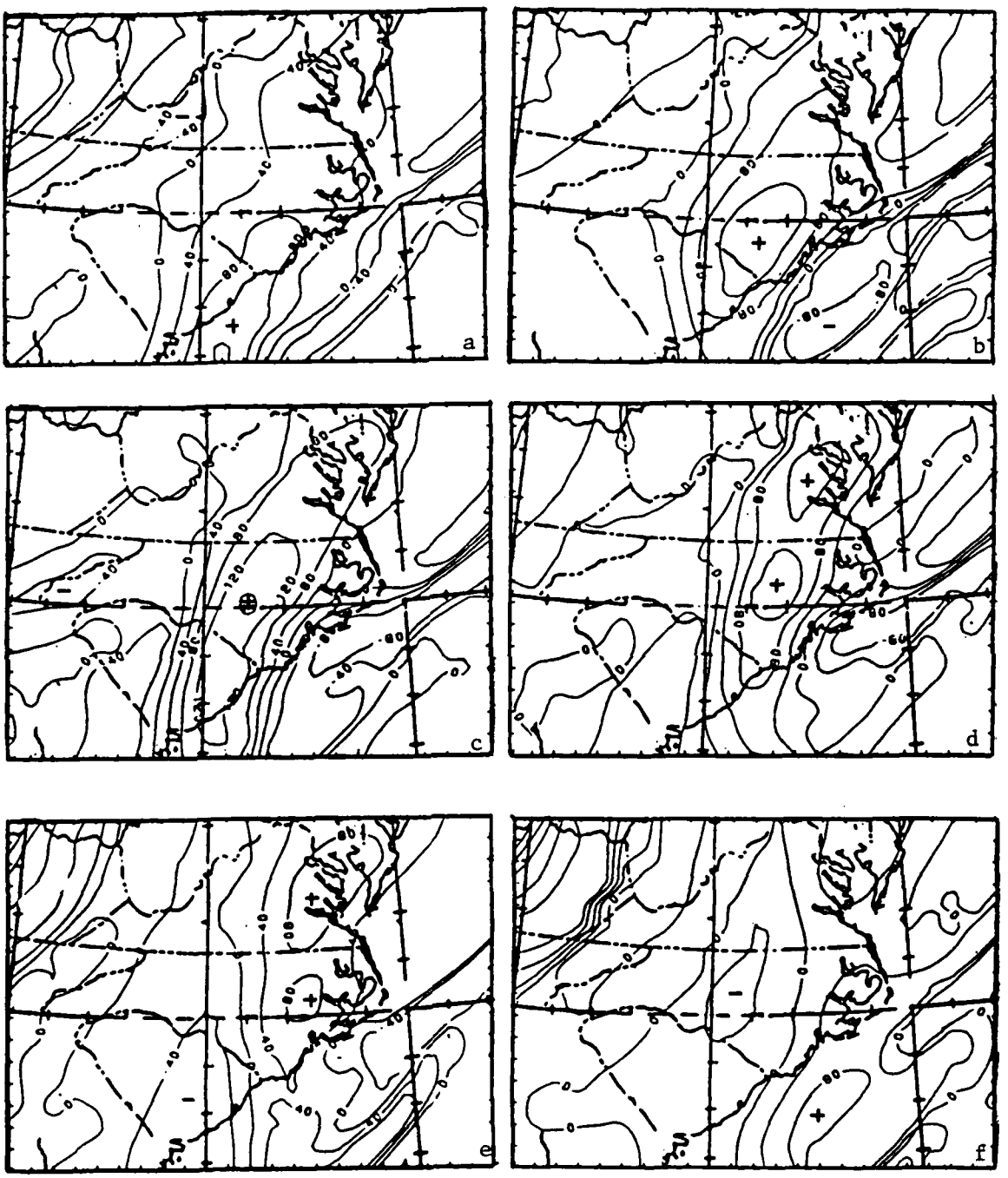


Figure 3.10. Eulerian frontogenesis for three-hourly periods from 0000 to 1500(a-f) GMT 22 December 1983. Units and contour interval are as in Figure 3.9. Positive values indicate frontogenesis.

temperature gradient maximum, the pattern predicts a westward movement of the frontal zone. The magnitude and location changes in the frontogenesis field physically represent the increasing coastal warm air advection clashing with the cold air advection developing over western South Carolina and resulting in a larger gradient of temperature advection.

At 0900 GMT the frontogenesis maximum shifts to eastern North Carolina as the cold air advection sweeps eastward across South Carolina and into central North Carolina. This illustration verifies the offshore frontal movement along the South Carolina coast and frontal intensification with slight eastward movement over North Carolina. The 1200 GMT and 1500 GMT pattern indicate further eastward movement and decrease in magnitude of frontogenesis. This is a direct response to a westerly flow which develops over the region, resulting in the extension of cold air advection all the way to the coastline of North Carolina.

Figure 3.11 represents the actual local rate of change of the temperature gradient, as calculated from the Barnes analyzed fields, for 0900 and 1200 GMT. These values are obtained by subtracting the temperature gradient values at four-hour intervals (two hours on either side of the specified time period). Comparing these fields with the Eulerian frontogenesis fields in Figure 3.10 it is clear that the Eulerian calculations are predicting too large a

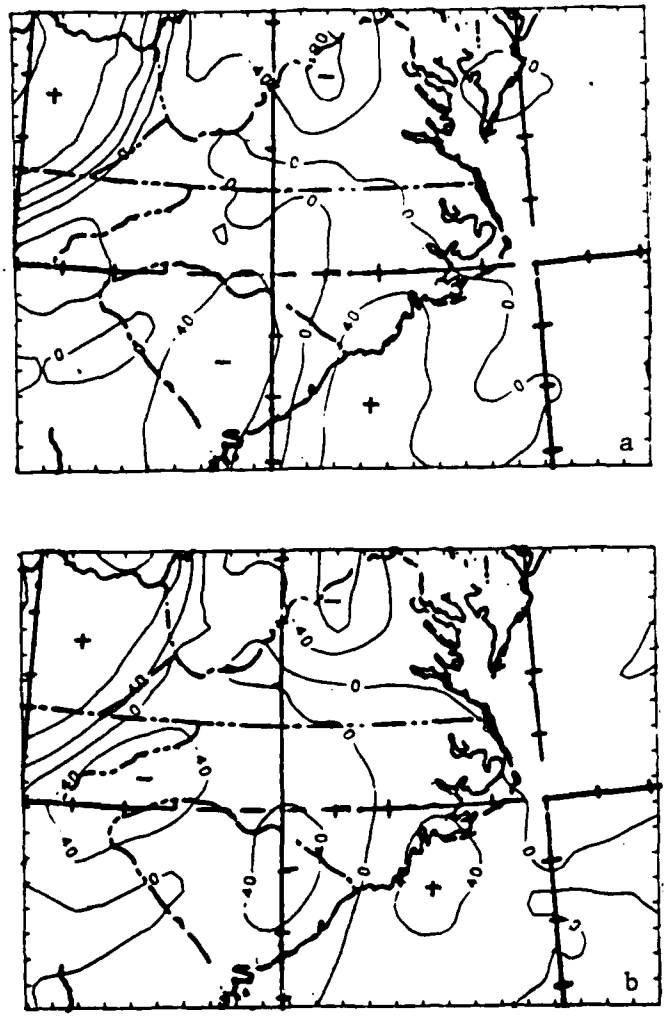


Figure 3.11. Actual local change of the temperature gradient for 0900 GMT(a) and 1200 GMT(b) 22 December. Units are as in Figure 3.9. Contour interval is every 40 units. Positive values indicate an increase in the temperature gradient.

temperature gradient increase in the frontal zone. Another interesting feature is that both the Lagrangian and Eulerian equations predict frontogenesis yet the temperature gradient patterns(Fig. 3.8) do not show any significant change. The time limit over which these values are calculated may be the cause of this discrepancy. The frontogenesis calculations are instantaneous values, however, the actual change in the temperature gradient is a result of a four-hour time differential calculation. Considering that the front moved inland and then retreated during this time, a major shift in the temperature gradient maximum probably would not appear.

3.5 Vertical Structure of the Coastal Front

Figure 3.12 illustrates vertical soundings for several locations in the region of the coastal front. The soundings of stations on the cold air side of the front are characterized by a strong temperature inversion below 900 mb. For example, the 1200 GMT 22 December sounding at Charleston reveals a 6.5 K temperature increase between the 989 mb and 974 mb levels. Calculations using the hypsometric relationship convert this to approximately a 1 K/20 meter vertical temperature gradient. The cold wedge clearly creates a highly stable lower boundary layer which partially accounts for the persistent nature of this phenomena.

The potential temperature cross section in Figure 3.13 provides additional information about the three-dimensional

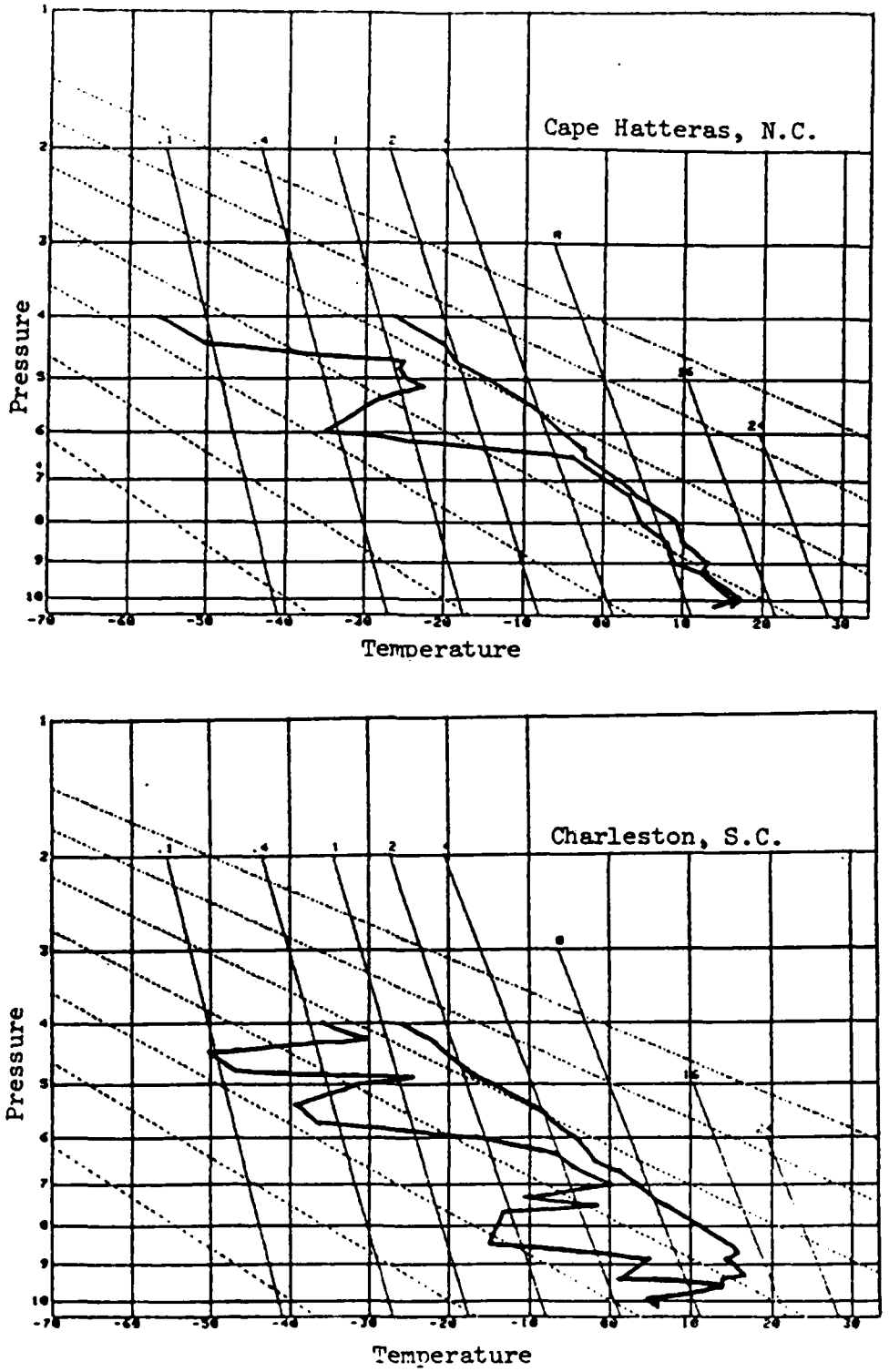


Figure 3.12. Stuve diagrams of temperature and dew point at Cape Hatteras and Charleston for 1200 GMT 22 December 1983. Pressure in $10^2$ mb and temperature in $^{o}C$.

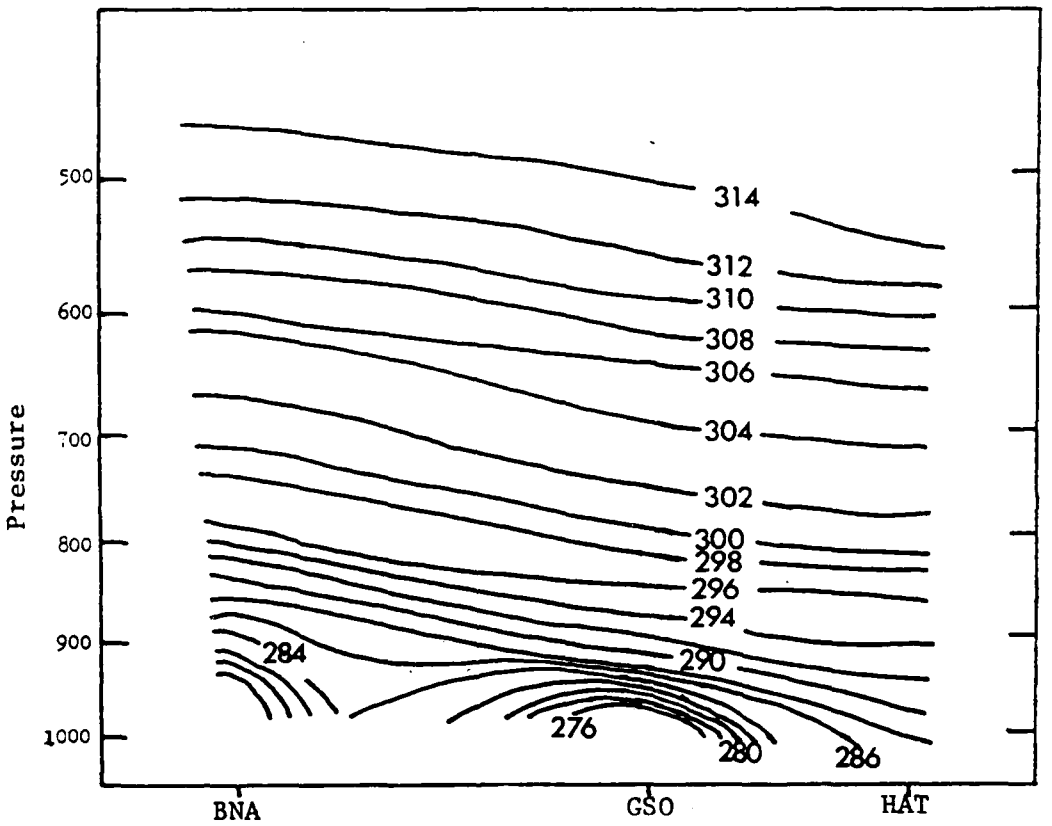


Figure 3.13. Cross section of potential temperature from Cape Hatteras to Nashville at 1200 GMT 22 December. Temperature interval is every 2 K.

framework of this coastal front. Although the overall pattern suggests generally warmer temperatures along the coastal region in contrast to the temperatures west of the Appalachians, the mesoscale structure of the coastal front is the most prominent feature of the analysis. The thermal structure of the front is characterized by the intense horizontal temperature gradient midway between Cape Hatteras and Greensboro. This intense temperature gradient extends vertically up to approximately the 925 mb level. The maximum depth of the cold air appears to exist at or near Greensboro. This is consistent with the previous location of the anticyclonic bulge in the surface pressure pattern since the anticyclonic bulge is a physical representation of the depth of the cold air.

Equation 2.4 (Section 2.2) is used to evaluate the three-dimensional frontogenetical patterns associated with the coastal front. All terms except the diabatic term are estimated. Gridded fields for each term were derived using the grid shown in Fig. 2.1. Values were calculated at the same levels specified in Section 2.4. Values were then transposed to the cross sections. Frontogenetical values were computed using 0000 GMT 22 December data, however, the frontogenetical patterns revealed little in comparison with the 1200 GMT data.

Figure 3.14a - 3.14d illustrate the frontogenetical fields for the HAT to Nashville, TN(BNA) cross section.

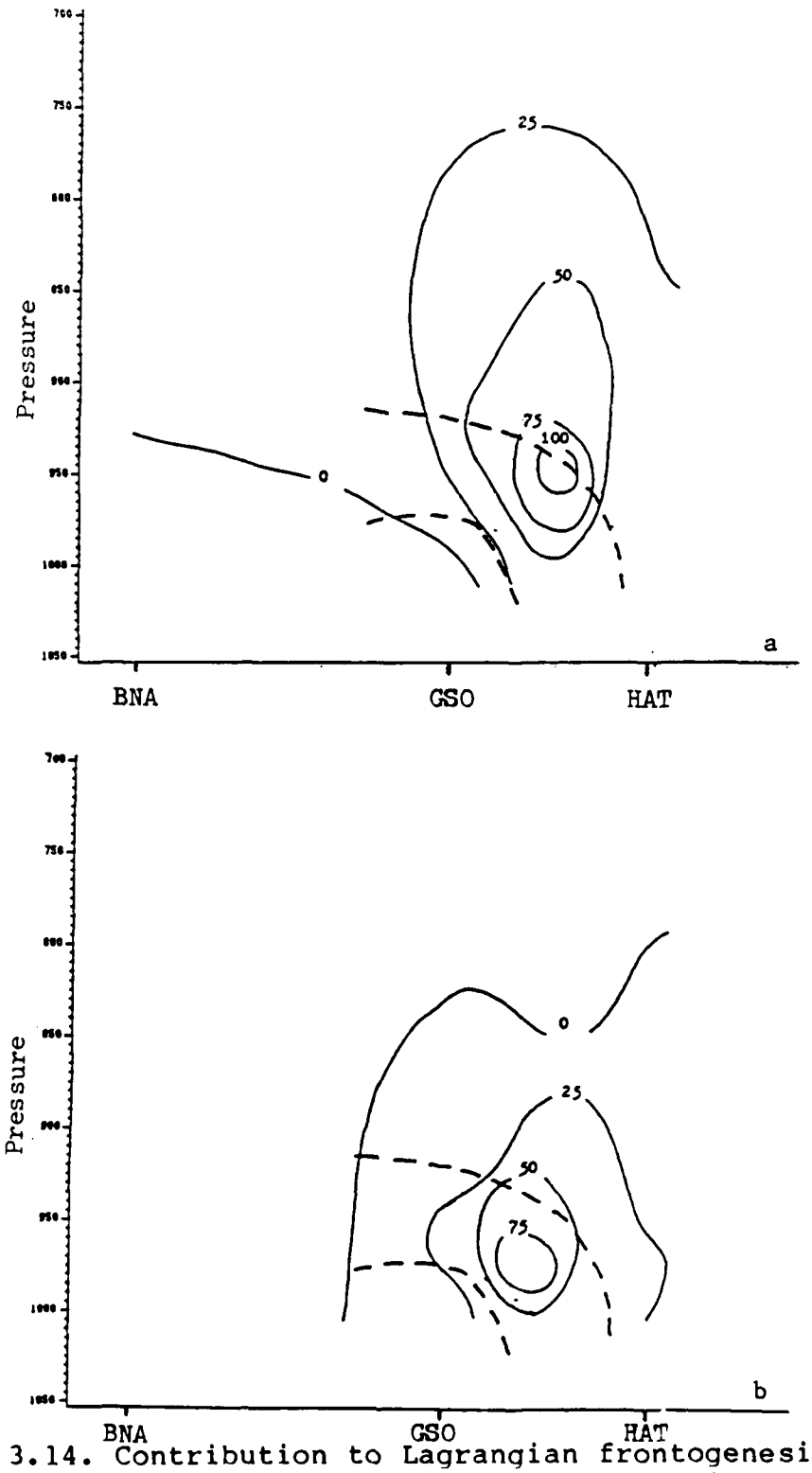


Figure 3.14. Contribution to Lagrangian frontogenesis from confluence(a), shear(b), and tilting(c) terms and sum(d) of a, b and c at 1200 GMT 22 December 1983. Dashed lines are 276 K and 288 K potential temperature lines.

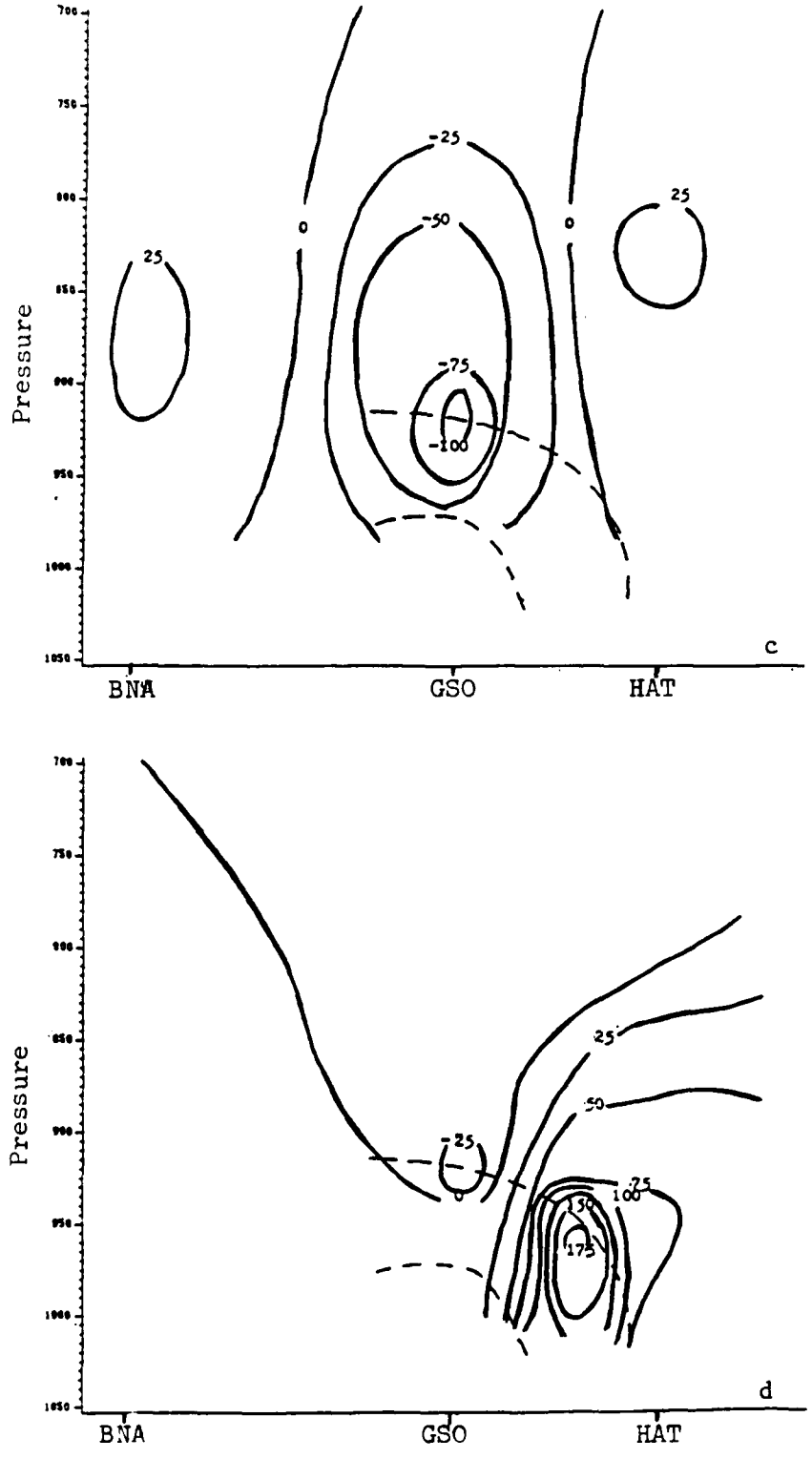


Figure 3.14. (continued)

Horizontal confluence (Figure 3.14a) and horizontal shear (Figure 3.14b) are frontogenetical within the frontal zone with maximum confluence values just above the 950 mb level and the maximum shear contribution just below 950 mb. The horizontal gradient of vertical velocity ("tilting") term is predominately frontolytical within the frontal zone with the maximum frontolytic contribution located west of the frontogenesis maximums of the shear and confluence terms. Although the magnitudes are not the same, these results do resemble the frontogenesis patterns of the coastal front study by Bosart(1981) and of the intense surface cold front study by Sanders(1955).

The wind components perpendicular and parallel to the HAT to BNA cross section are shown in Figure 3.15. The patterns display a strong confluence and shear, respectively, at the 950 mb level. Within the coastal front zone, the winds are predominately from the north and west, while the winds outside the frontal zone are mostly from the south and east. Particularly striking is the manner in which the winds perpendicular to the cross section slope with and give additional definition to the top of the frontal zone. The frontal zone clearly separates the colder northerly flow from the warmer southerly flow.

The strongly convergent flow at the eastern edge of the frontal boundary suggests strong vertical motions within the frontal zone. Vertical velocities were derived using the

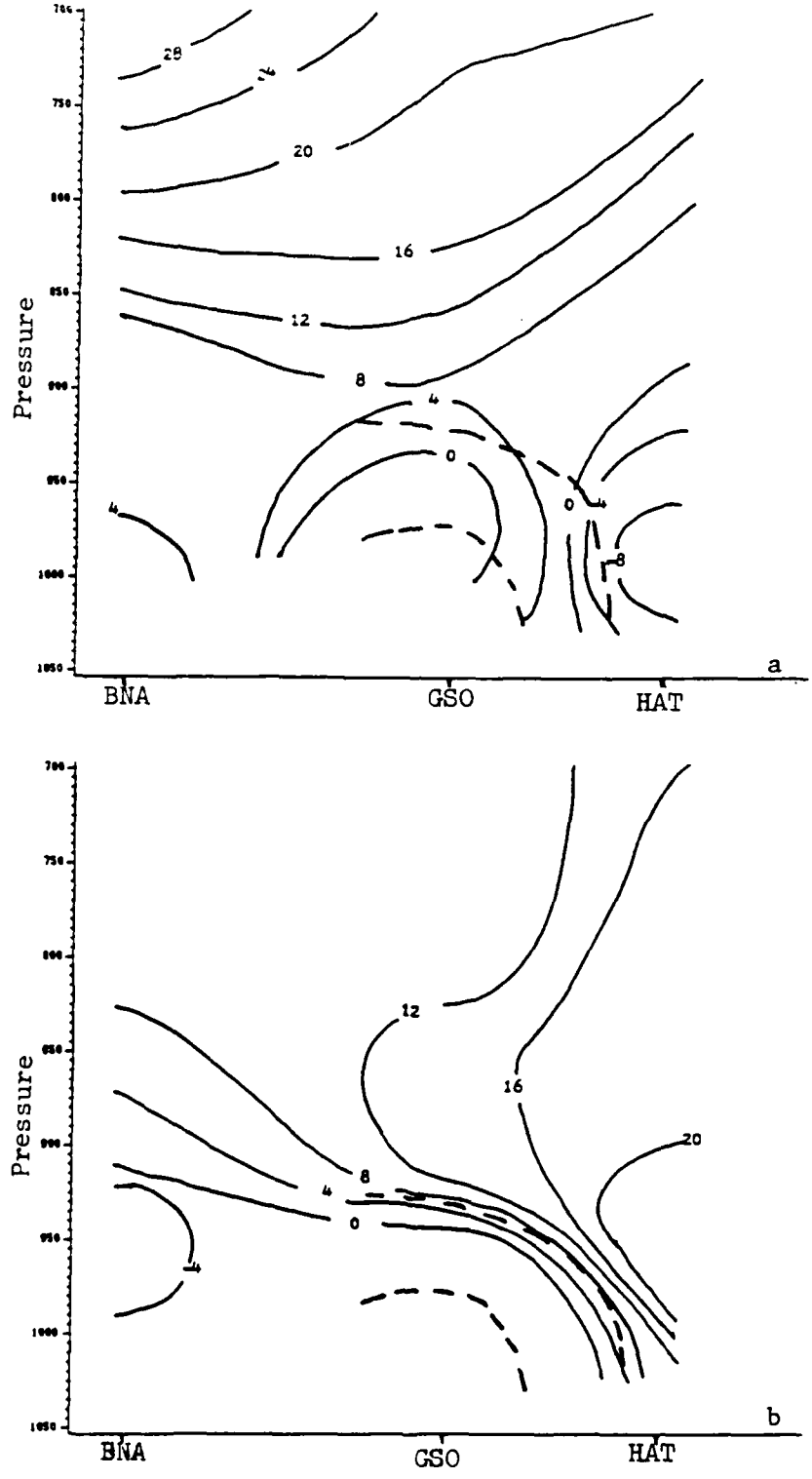


Figure 3.15. Wind speeds parallel(a) and perpendicular(b) to the cross section at 1200 GMT 22 December. Positive values are a west(a) and south(b) wind. Dashed lines are as in Fig. 3.14. Units are in ms-1.

kinematic method outlined in Section 2.3. Figures 3.16 and 3.17 illustrate the vertical velocity patterns for 0000 GMT and 1200 GMT 22 December along the HAT to BNA cross section as well as the Wallops Island, VA(WAL) to Dayton, OH(DAY) cross section. Both cross sections indicate negligible vertical velocities along the coastal region at 0000 GMT, however, the 1200 GMT patterns display a markedly different configuration. Ascent of about 2-3 x $10^{-3}$ mb $s^{-1}$ extends into the upper levels of the coastal front zone. The ascending motion at the lower levels is apparently an extension of the ascending motion located at higher levels. This suggests that the vertical motions within the zone is not solely caused by the convergence within the frontal zone, but, may be characteristic of the broader scale low and mid-tropospheric flow pattern. These results are somewhat contradictory to the results of Bosart(1981) in which a separate and distince region of strong ascent, in excess of 12 x $10^{-3}$ mb $s^{-1}$, within the frontal zone. Although the ascending motion is not as distinct as in the case investigated by Bosart, the general circulation within this coastal front is characteristic of the thermally direct circulation discussed by Bosart. The air in the warm sector rises as it passes above the cold air and the cold air at the surface flows back toward the warm sector.

## 3.6 Precipitation Analysis

Fig. 3.18 illustrates the six-hourly precipitation

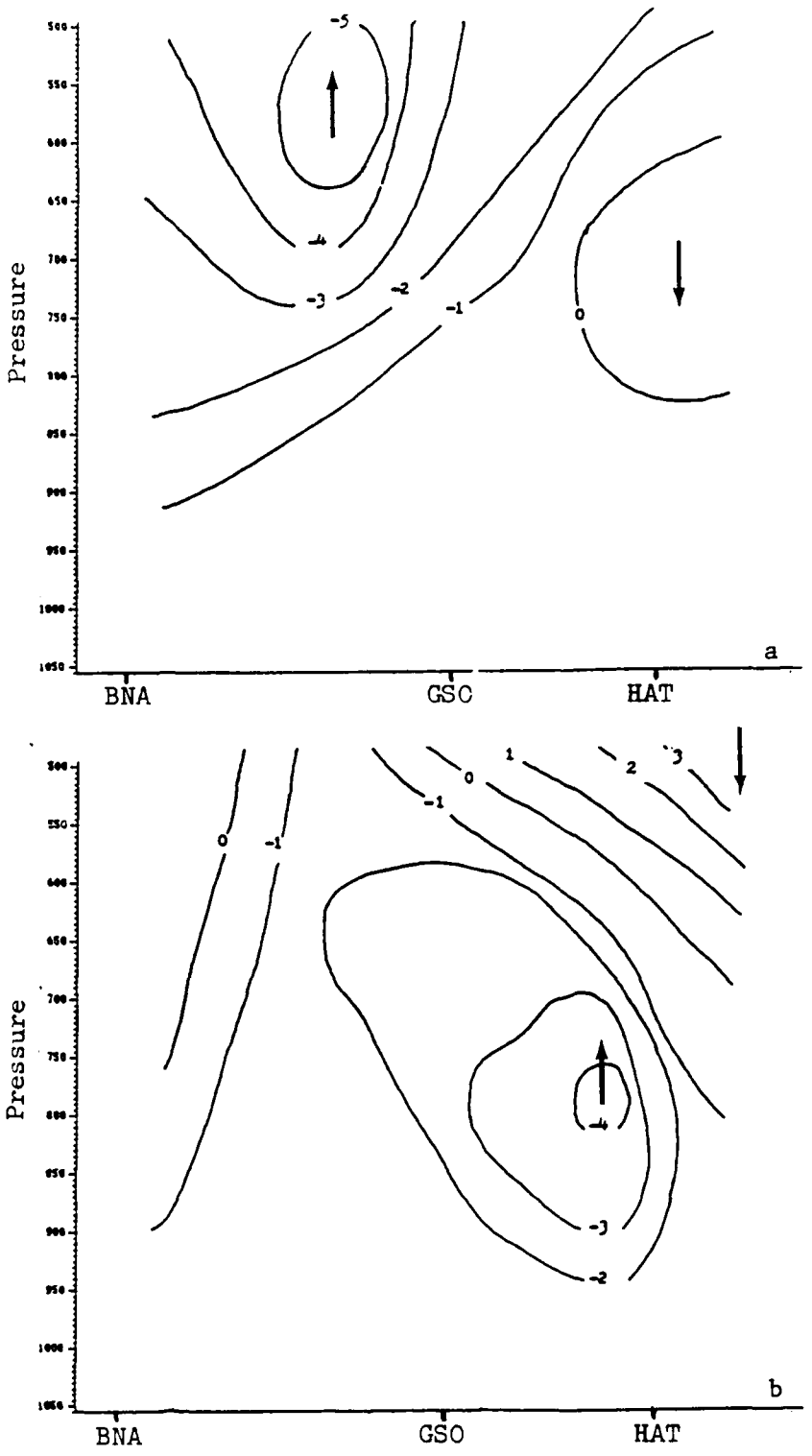


Figure 3.16. Vertical motion along the Cape Hatteras to Nashville cross section at 0000 GMT(a) and 1200 GMT(b) 22 December. Units are $10^{-3}$ mb $s^{-1}$.

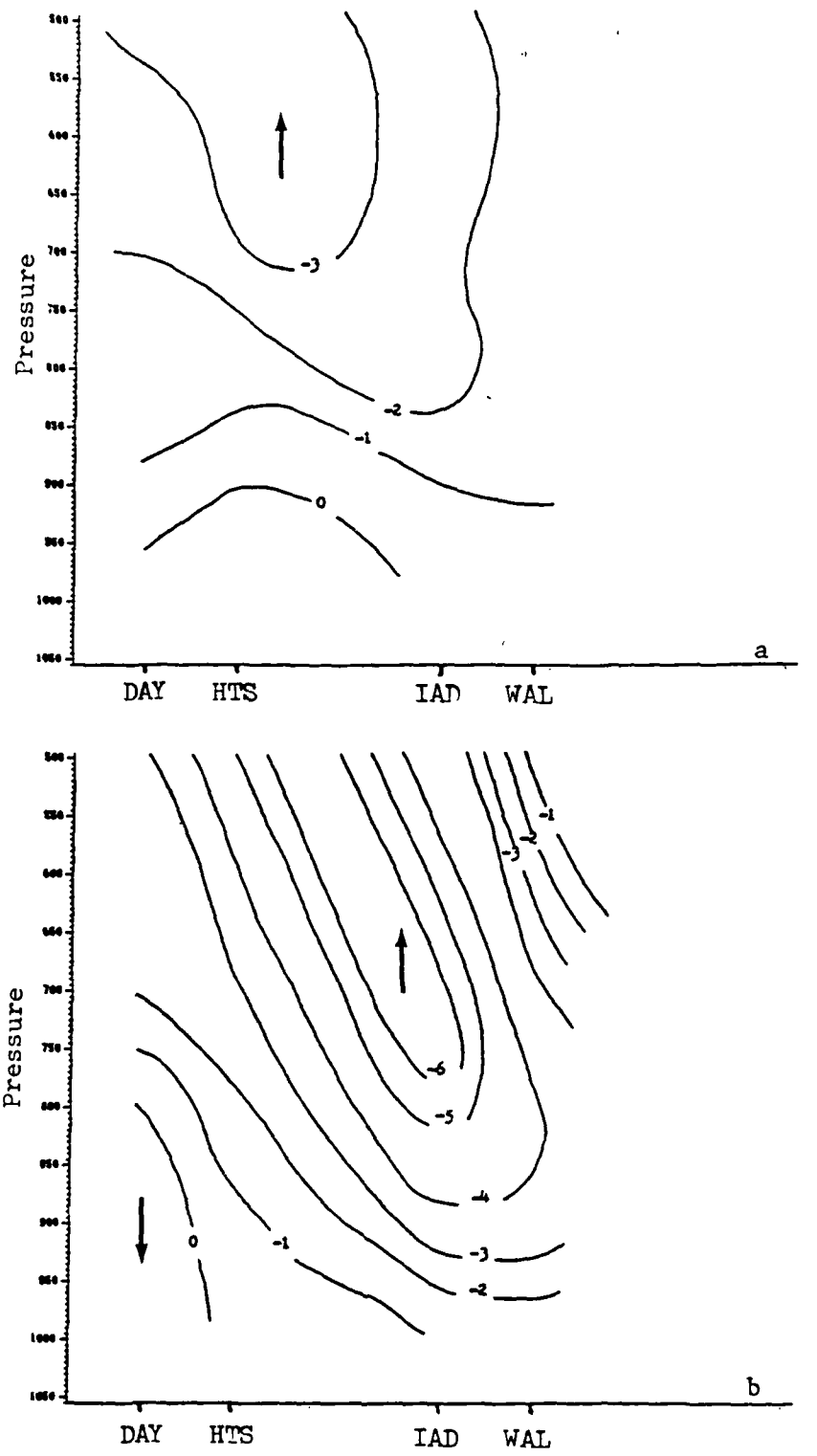


Figure 3.17. Vertical motions along the Wallops Island to Dayton cross section for 0000 GMT(a) and 1200 GMT(b) 22 December. Units are same as Figure 3.16.

totals for designated periods. An orderly progression of the precipitation maximum from western North Carolina to southwestern New Jersey is evident. The maximum over western North Carolina probably reflects some orographic effects. Northeast and easterly winds through 0600 GMT undoubtably resulted in some lifting up the mountain slopes and higher precipitation totals. This assumption is further substantiated by the 1200 GMT totals which indicate little precipitation over the same area when northwesterly winds dominated.

The advancement of the large scale precipitation maximum is consistent with the vertical velocity patterns illustrated in Figs. 3.16 and 3.17. The strongest vertical velocities are between BNA and Greensboro, NC(GSO) at 0000 GMT 22 December, however, the vertical velocity maximum shifts northeastward to the vicinity of Washington, DC(IAD) by 1200 GMT. The high correlation between the precipitation and vertical velocity maximums instills confidence that the vertical velocity computations are representative of the atmospheric motion.

Bosart(1972,1975,1981) and Marks and Austin(1979) identify the cold air side of the coastal front zone as favorable for precipitation enhancement. Figure 3.18 seems to indicate similar results. In Fig. 3.18(a), a maximum extends through central South Carolina while in Fig. 3.18(b), a maximum is evident from eastern Virginia

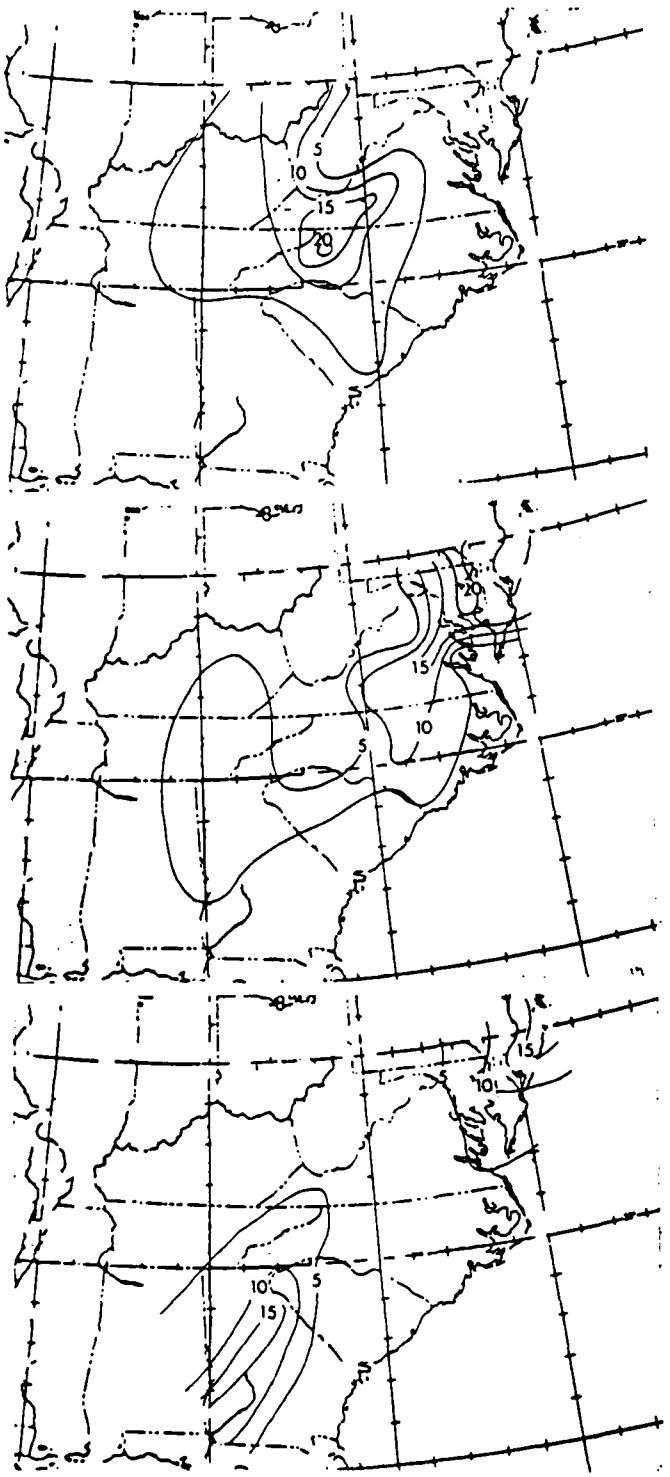


Figure 3.18. Six-hourly precipitation totals for period ending 0600 GMT(top), 1200 GMT(center), and 1800 GMT(bottom) 22 December 1983. Units are mm.

southward through east central North Carolina. Both of these maxima are located near the edge of the farthest inland penetration of the coastal front.

Radar observations were also reviewed to study the characteristics of the precipitation field. Radar films and recorded observations from CHS, Wilmington, NC(WIL), HAT and Patuxent River, MD(NHK) were analyzed. In an attempt to identify precipitation enhancement, individual cells and band movements were analyzed in conjunction with hourly precipitation reports. Inconsistencies in reporting accuracies and location of precipitation in relation to reporting stations prevented the development of any conclusions concerning the enhancement of precipitation as a cell or band passed through the coastal front zone.

At 0000 GMT 22 December 1983, the CHS radar indicated a broad region of light precipitation. The echo pattern was characteristic of stratiform precipitation with few intensities above 3 mm $hr^{-1}$. Between 0440 GMT and 0520 GMT, a broken line of echoes developed into a solid line of showers with embedded convective activity. The line extended 100 Km southward from a point 20 Km east of CHS. Fig. 3.19 illustrates how this line progressed eastward and embedded convective cells developed. The band was apparently frontal activity associated with the eastward movement of the convergence zone associated with the coastal front.

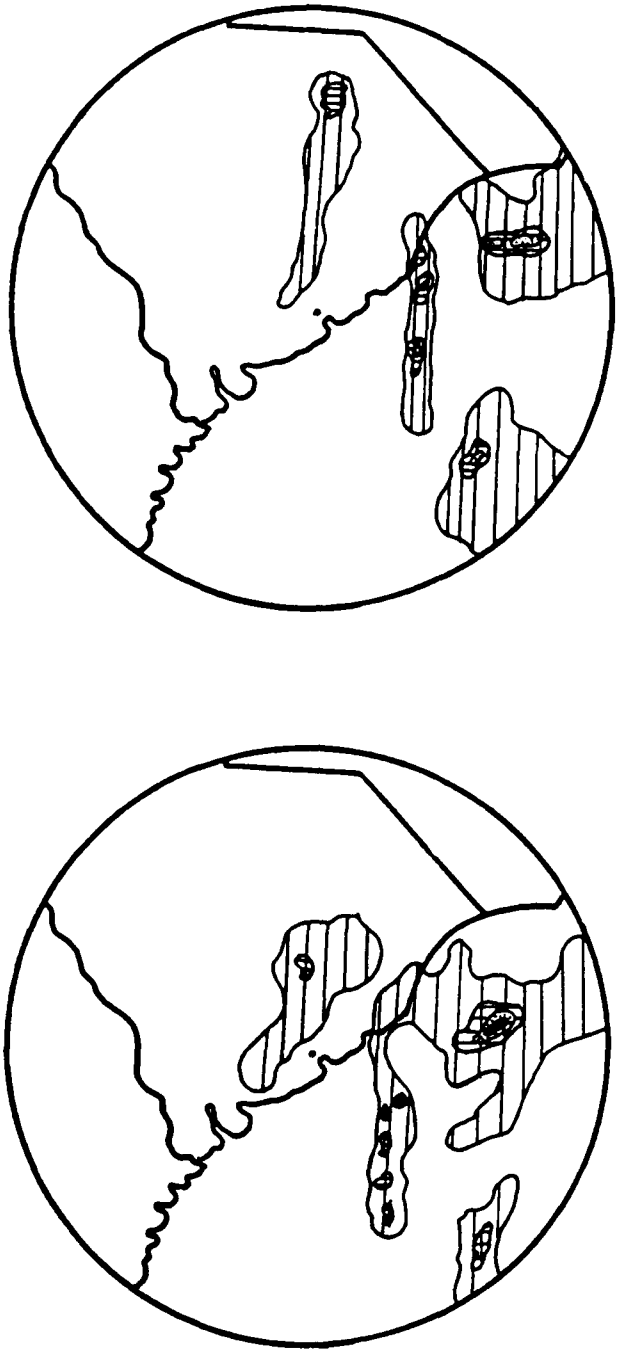

Figure 3.19. Simulation of radar PPI scope at Charleston at 0530 GMT(top) and 0630 GMT(bottom) 22 December. VIP levels are illustrated as follows: 1(hatched), 2(cross-hatched), 3(dotted), 4(black).

Analysis of the WIL and HAT radars indicates small cells of convective activity. The pattern was somewhat random and had no correlation with the inland movement of the coastal front. However, a small line of showers did develop around 0700 GMT, southwest of WIL, and progressed eastward. This was probably an extension of the line which developed east of CHS a few hours earlier.

The most interesting radar observations were at NHK. Several distinct bands developed over eastern Virginia and progressed northeastward at about 20 m $s^{-1}$. The bands often expanded as they moved northeastward and frequently merged with other areas of precipitation in the northern and eastern region of radar coverage. Figure 3.20 illustrates a few of these bands. Associated rainfall rates were on the order of 10-20 mm $hr^{-1}$, which is consistent with the larger vertical velocities and observed rainfall amounts in this region.

A conection between mesoscale rainbands like those identified on the NHK radar and convective instability was established by Kreitzberg and Brown(1970). Marks and Austin used those concepts to link rain bands with coastal front precipitation. Figure 3.21 presents vertical profiles of equivalent potential temperature for HAT, GSO, CHS, and IAD respectively. The GSO and CHS temperature profiles are quite similar to the profiles presented by Marks and Austin. An inversion layer is capped by a deep layer of warmer, more

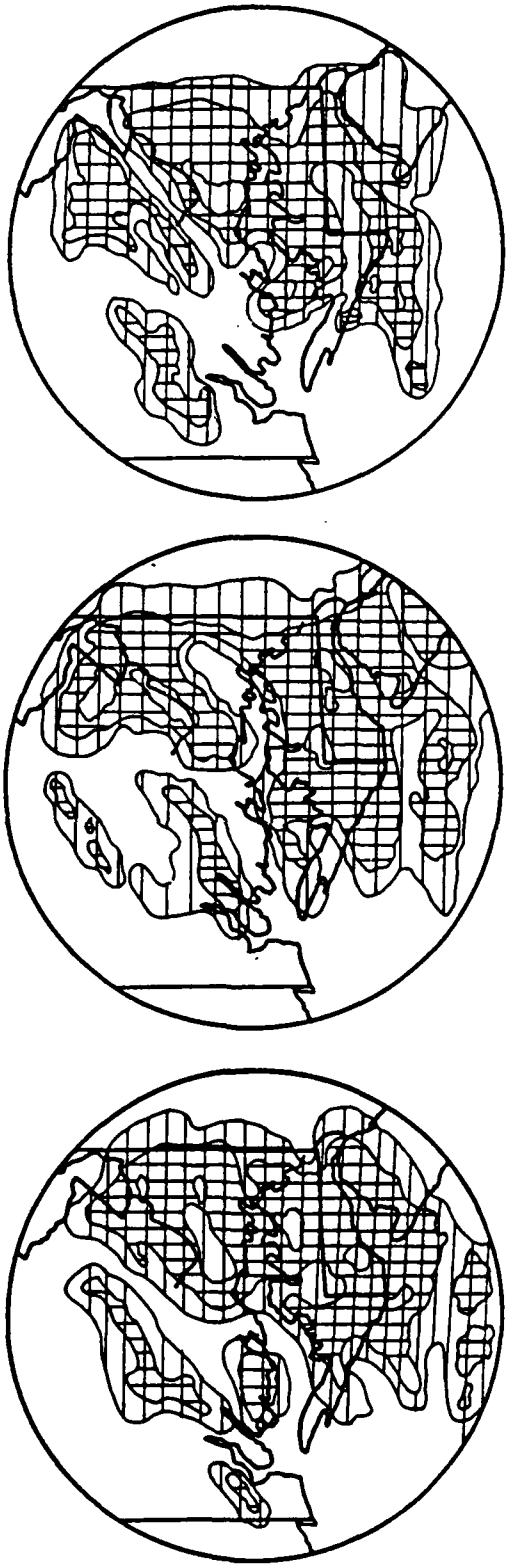

Figure 3.20. Same as Figure 3.19 except at Patuxent River, Md. at 0915 GMT(top), 0945 GMT(center) and 1015 GMT(bottom) 22 December.

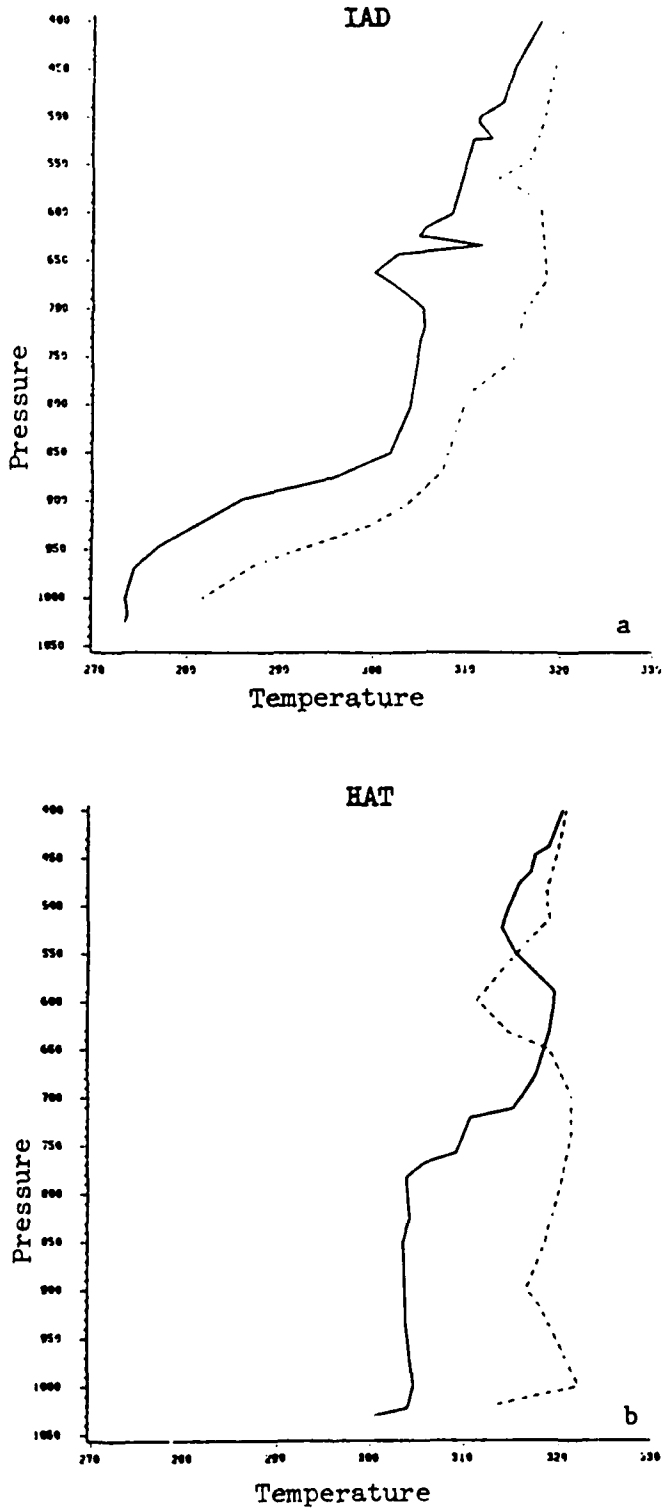


Figure 3.21. Vertical profiles of equivalent potential temperature at 0000 GMT (solid) and 1200 GMT (dashed) 22 December at Washington, D.C.(a), Cape Hatteras(b), Greensboro(c) and Charleston(d).

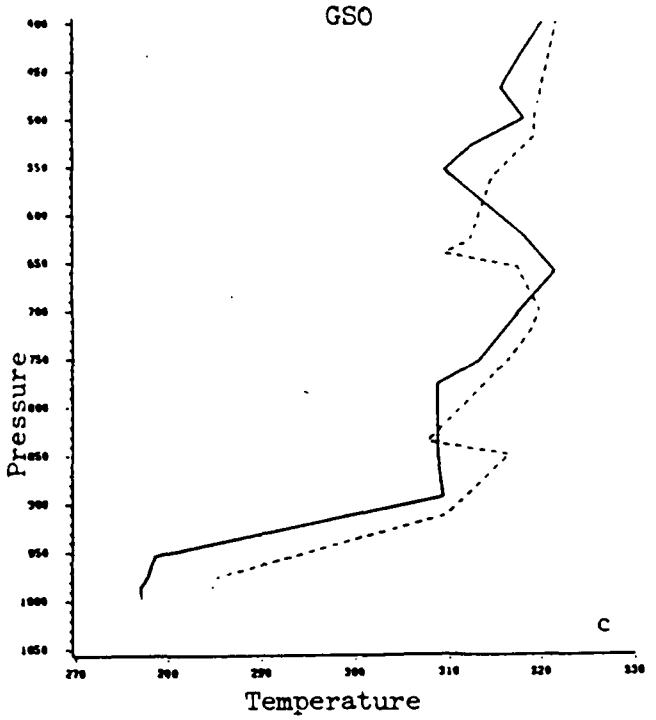


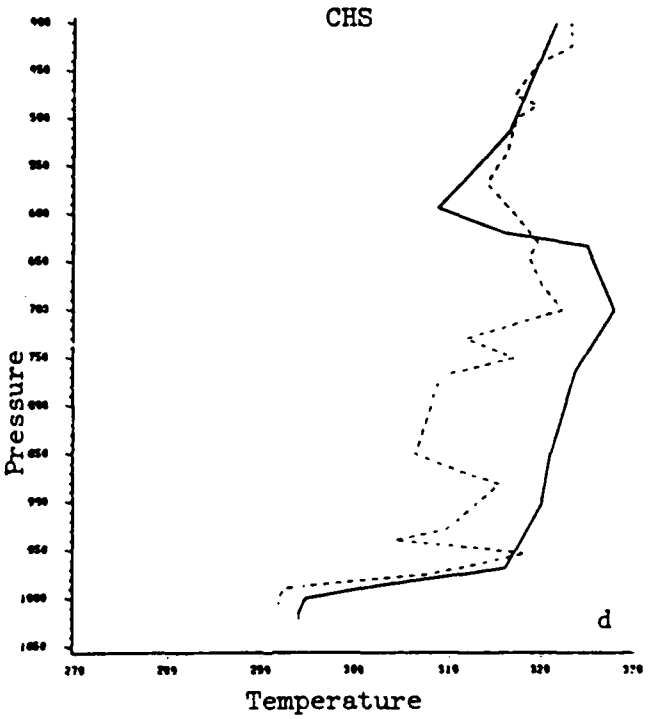


Figure 3.21. (continued)

stable air. Above the warmer air, a convectively unstable layer of about 100 mb depth is evident. The HAT profile displays different characteristics since this station is within the warm air. Warm air extends up to the 650 mb level where a convectively unstable layer begins and extends to the 580 mb level. The convectively unstable layers at IAD are much more shallow and are of lesser magnitude.

At 1200 GMT, the unstable layers have mostly decreased in depth and magnitude although distinct unstable layers clearly exist at HAT, GSO and CHS. On the contrary, the unstable layer at IAD was very shallow(about 20 mb). In studying these profiles, it is evident that the HAT, GSO and CHS unstable layers are deeper and apparently more unstable than the layer at IAD, yet the precipitation totals were significantly higher at the latter station. These profiles suggest that greater amounts of precipitation might be expected at the more southern stations; however, upward vertical motion must exist at the level of instability in order for it to have any effect upon the vertical velocities. Figures 3.16(b) and 3.17(b) indicate that little upward vertical velocity exists at the instability level at three southern stations while at IAD strong rising motion exists at the level of instability. It is possible that the upward vertical motion at IAD leads to the realization of the covective instability thus creating a more shallow layer of instability.

Fig. 3.22 illustrates the wind components parallel and perpendicular to the movement of the precipitation fields at HAT and IAD. The v-component (perpendicular to the band movement) has a value of zero at the steering level of the precipitation. At both stations the steering level is associated with the base of the convectively unstable layer. These results are consistent with the previous findings of Marks and Austin and suggests a relationship between the convective instability and the precipitation fields.

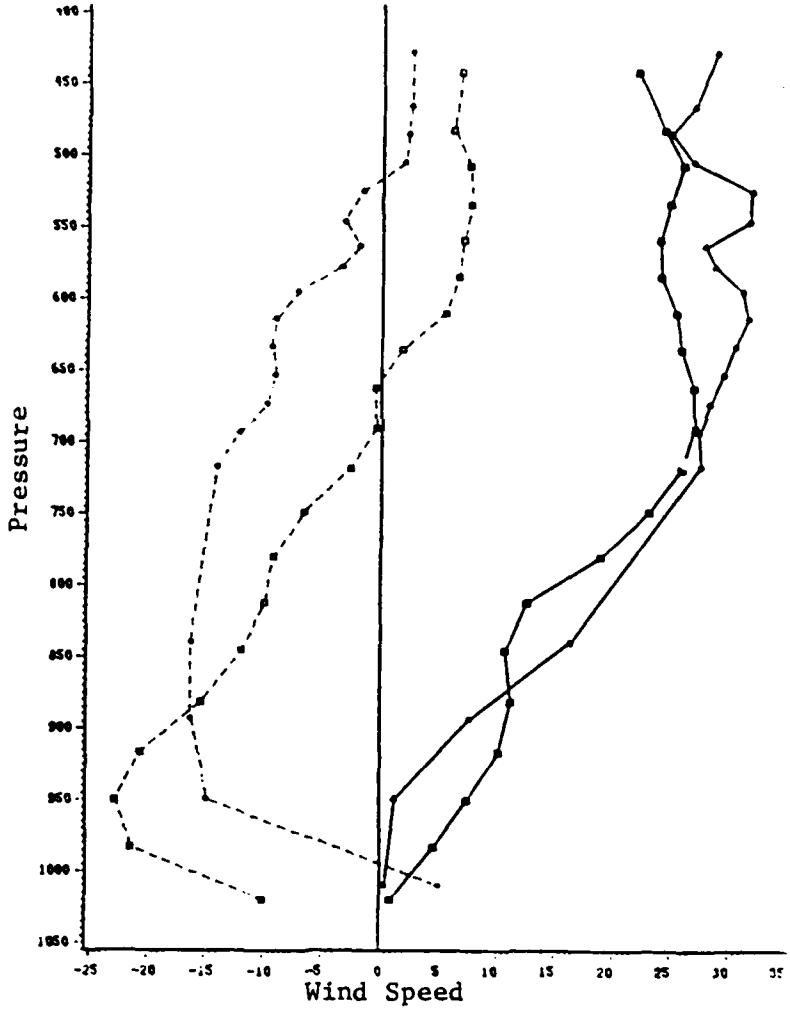


Figure 3.22. Wind components perpendicular(dashed) and parallel(solid) to precipitation band movement for Cape Hatteras (filled circle) and Washington, D.C.(square) at 1200 GMT 22 December. Wind speeds in units of m $s^{-1}$.

# 4. Geostrophic Winds and the Cold Wedge

## 4.1 Alternative Geostrophic Wind Computation Methods

The horizontal pressure pattern is of the utmost importance in producing horizontal atmospheric motions, however, in mountainous terrain, sea level pressure patterns may not accurately depict the correct pressure gradients. The errors are largely a result of the twelve-hour mean temperature factor used to reduce pressure values to sea level and the empirical terms added to pressures above 1000 ft. Saucier(1955) indicates that errors may be as great as 10mb at high elevations while neighboring stations above and below 1000 ft. may have pressure differences as much as 0.5mb.

These pressure errors often result in erroneous surface geostrophic wind calculations. To combat this problem, Sangster(1960) developed a new method to compute the pressure gradient force on a non-isobaric surface. The method is based upon a reference surface which is a highly smoothed representation of the earth's terrain. Using this surface requires the reduction(both upward and downward) of surface pressures to the reference level. Sangster claimed this method reduced the errors since most pressure reductions were minimal when compared to the pressure reductions to sea level from high elevations.

Sangster expressed the pressure gradient force as an additive function of a geostrophic stream function and a

geostrophic potential function. His test results indicated that the smoothed terrain geostrophic winds in mountainous regions were often more accurate than the geostrophic winds assessed from the sea level pressure pattern. His method was most effective in synoptic situations when cold air bordered along a mountain range. In these scenarios, extreme sea level isobar concentration suggested strong geostrophic winds yet the actual winds were relatively light.

Richwein(1980) examined the ineffectiveness of sea level isobars to reflect the wind flow in a cold wedge east of the Appalachians. He employed a technique for calculating surface geostrophic winds based upon the thermal wind relationship, where the thermal wind is the geostrophic wind at a lower level subtracted from the geostrophic wind at an upper level. Assuming the 850 mb level to be a suitable upper geostophic level, Richwein subtracted calculated thermal winds from the 850mb winds to obtain surface geostrophic winds. The results are remarkably similar to the actual surface winds in a cold wedge.

Richwein then related this theory to coastal frontogenesis. Prior to frontogenesis, the horizontal temperature gradient is relatively small resulting in a small thermal wind. Adding the thermal wind to the surface wind produced a light northeast 850 mb wind. This result is consistent with the early period of a cold wedge. At the

mature stage of frontogenesis, the horizontal temperature gradient has increased significantly resulting in a strong thermal wind. Vectorially adding this thermal wind to the surface wind results in a southerly 850 mb wind. This southerly 850 mb wind is consistent with the veering of 850 mb winds during the onset of frontogenesis.

4.2 A Variation of the Sangster Model

Geostrophic wind computations within the cold wedge are generally poor estimators of the actual wind flow. Bosart(1975) attributes the ageostrophy to differential friction effects. Richwein and Sangster argue that sea level pressure patterns do not accurately depict the horizontal pressure gradient in mountainous terrain. To further investigate this problem, modifications are made to the Sangster model to test the hypothesis that pressure reductions are partially responsible for the apparent ageostrophy of the cold wedge wind pattern.

Equation 4.1 expresses the geostrophic wind normal to the isobar gradient.

$$V_g = -(1/\rho f) * \partial P/\partial n \qquad 4.1$$

where $\rho$=Density

f=coriolis parameter

$\partial P/\partial n$=horizontal pressure gradient

As mentioned earlier, the use of sea level pressures, in equation 4.1, can lead to errors in mountainous terrain. Sangster avoided this problem by creating a fictitious,

smoothed surface. Another option is to change the reference surface from mean sea level to a terrain level reference surface. By using the earth's terrain as a reference level, pressure reductions are totally avoided. This reference level is developed by calling the terrain surface $\sigma$ defined by:

$$\sigma = P/P_s$$

Here, P=pressure at a given level

$P_s$=station pressure

One sees that $\sigma$=1 at the earth's surface and is the reference surface aforementioned.

The horizontal pressure gradient on a $\sigma$-surface is mathematically derived through the use of the transformation equation expressed in Equation 4.2.

$$\nabla_r(Q) = \nabla_z(Q) + Q/\ z^*(\nabla_r(z)) \qquad 4.2$$

Using the new reference surface, where r= and Q=P, changes Equation 4.2 into Equation 4.3.

$$\nabla_\sigma(P) = \nabla_z(P) - p/\ z^*(\nabla_\sigma(z)) \qquad 4.3$$

Assuming a hydrostatic balance, Equation 4.3 becomes

$$(1/\rho)\nabla_z(P) = (1/\rho)\nabla_\sigma(P) + g\nabla_\sigma(z) \qquad 4.4$$

where g=acceleration of gravity.

The left hand side of 4.4 is the horizontal pressure gradient force on a constant height surface and is a function of the gradients of station pressure and elevation on a $\sigma$-surface.

In finite difference form, the horizontal pressure

gradient along the terrain slope becomes

$$(1/\rho)(dP/dn)_z=(1/\rho)(dP/dn)_\sigma+g(dz/dn)_\sigma \quad 4.5$$

Substituting Equation 4.5 into Equation 4.1 yields the geostrophic wind on a o-surface.

$$V_g(\sigma)=-(1/f)((1/\rho)\ P/\ n+g\ z/\ n)_\sigma \quad 4.6$$

4.3 Test Results of the Modified Sangster Method

The Barnes analysis scheme is used to create gridded values of station pressure and elevation. Since the pressure gradient is a function of both variables, consistent analyses demand that elevations are used for only stations which have available station pressures. This is a minor disadvantage to this method, since a new gridded elevation field is computed for every hourly data set. Considering the minor cost of the additional computations, this method is still much preferred to Sangster's more costly method of arbitrarily reducing pressures to a reference surface.

Figure 4.1 represents the Barnes gridded wind vectors at 12Z 21 December for surface winds, sea level geostrophic winds and terrain level geostrophic winds respectively. Both geostrophic wind fields display similar patterns and are in sharp contrast to the actual wind field. In particular, two discrepancies are readily visible. First, the geostrophic patterns indicate easterly flow over the coastal regions while northeast flow dominates the actual wind pattern. Second, the geostrophic winds quickly shift

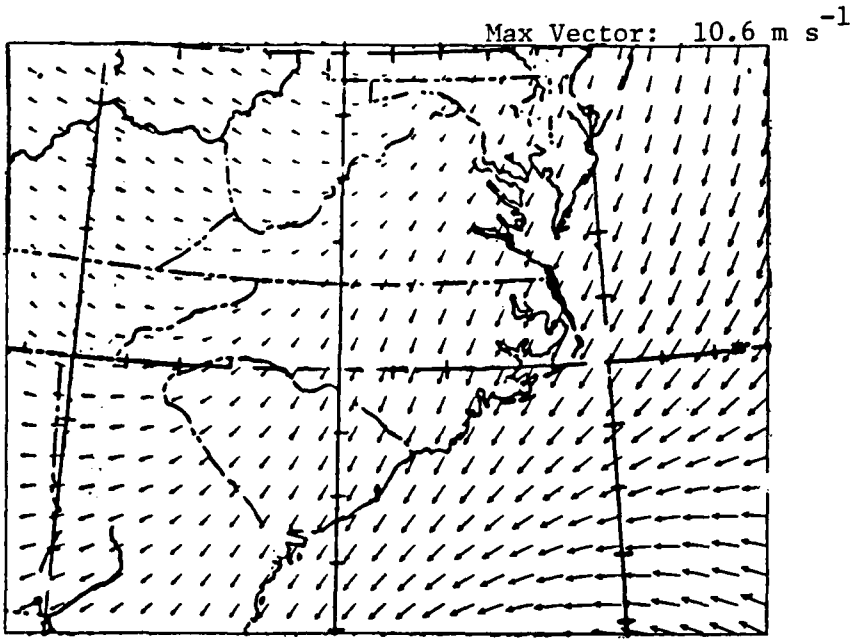


Figure 4.1. Barnes analyzed wind fields for actual winds(a), sea level geostrophic winds(b) and terrain level geostrophic winds(c) at 1200 GMT 21 December.

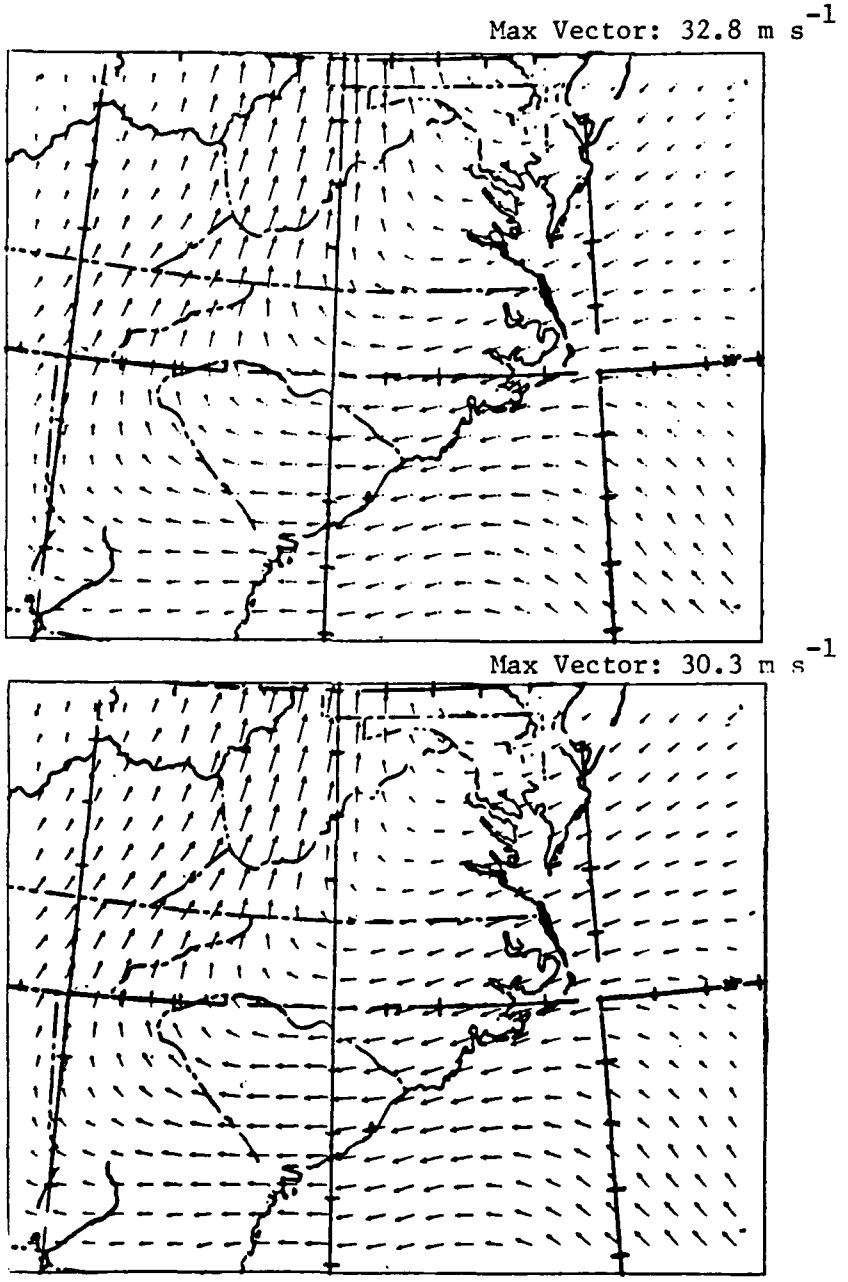


Figure 4.1. (continued)

to the south over the more elevated terrain while the actual wind field gradually shifts to the east and decreases in magnitude. These discrepancies are consistent with the sea level isobar pattern which is oriented east-west over the coastal region and is tightly packed in a north-south orientation against the mountains.

A more rigorous examination of the geostrophic fields reveal some minor variations between the patterns. The terrain following geostrophic winds are slower to shift to a southerly component in the vicinity of the anticyclonic axis. This variation may be a result of the gradient of elevation term. Over the coastal regions, the gradient of elevation is small and contributes little to $V_g(\sigma)$, however, along the mountain chain, the elevation gradient term is large and therefore has a greater impact upon the resultant winds.

To test the accuracy of both geostrophic winds in relation to the actual wind fields, Standard Errors(SE) are calculated over the entire region from the Appalachian mountains eastward. SE's are also calculated for just the mountainous region to determine if the $V_g(\sigma)$ calculations are more accurate over higher sloped terrain as is indicated by visual inspection. SE values were obtained by summing the difference of the specific geostrophic wind value from the Barnes gridded actual wind value. This particular method requires the assumption that the Barnes

gridded wind field represent the true wind field over the grid region. The results are tabulated in Table 4.1 and 4.2.

Standard error values indicate that $V_g(\sigma)$ calculations over the highly sloped terrain are slightly more accurate than over the region as a whole. The u-component (north-south) errors for terrain level winds are as much as 5.5 m/s less than the geostrophic winds over the sloped terrain. Over the region as a whole, the u-component errors only differed by 1-3 m/s. Of much greater significance are the overall magnitudes of the SE's which range from 6-15 m/s. Since winds in the cold wedge rarely exceed 7 m/s, it is clear that neither method is satisfactory for predicting the observed wind pattern.

To insure that density calculations were not influencing the wind computation, density values were obtained through two separate methods. Density values for the case above were calculated at every grid point using the equation of state. The alternative method calculated desity values at each station and allowed the Barnes scheme to create a gridded density field. The results of the alternative method were very similar to the original method.

Table 4.1. Mean values of u and v components of true wind field and standard errors for u and v components of sea level geostrophic winds(G) and terrain following geostrophic winds( ) over sloped terrain only. Units are m $s^{-1}$. Times are GMT.

| TIME/DATE | U | V | U(G) | V(G) | U( ) | V( ) |
|---|---|---|---|---|---|---|
| 0600 21 Dec | 2.6 | 2.7 | 12.6 | 6.4 | 10.5 | 6.7 |
| 0900 21 Dec | 2.3 | 2.8 | 13.3 | 7.0 | 11.1 | 7.4 |
| 1200 21 Dec | 2.8 | 2.5 | 15.0 | 7.7 | 9.5 | 9.0 |
| 1500 21 Dec | 2.8 | 3.0 | 14.8 | 7.2 | 9.7 | 7.8 |
| 1800 21 Dec | 2.5 | 2.9 | 14.4 | 7.6 | 9.5 | 8.8 |

Table 4.2 Mean values of u and v components of true wind field and standard errors for u and v wind components of sea level geostrophic winds(G) and terrain following geostrophic winds( ) over all terrain. Units are m $s^{-1}$. Times are GMT.

| TIME/DATE | U | V | U(G) | V(G) | U( ) | V( ) |
|---|---|---|---|---|---|---|
| 0600 21 Dec | 3.7 | 2.4 | 9.5 | 9.5 | 8.2 | 9.2 |
| 0900 21 Dec | 3.6 | 2.5 | 10.0 | 10.4 | 8.6 | 10.1 |
| 1200 21 Dec | 4.0 | 2.6 | 11.0 | 11.3 | 8.5 | 11.6 |
| 1500 21 Dec | 3.6 | 3.2 | 11.0 | 9.8 | 8.4 | 9.4 |
| 1800 21 Dec | 3.0 | 3.5 | 10.8 | 10.6 | 8.0 | 11.6 |

## 5. Summary and Conclusions

Analysis of surface data over the mid-Atlantic states during December 21-22, 1983, revealed several characteristics associated with the development of a coastal front. A shallow dome of cold air wedged against the southern Appalachiar · resulted in a persistent anticyclonic bulge east of the mountain chain. Light northerly(ageostrophic) flow within the bulge resulted in light cold air advection while southeasterly winds over the Atlantic produced strong warm air advection into the coastline region. The net effect of these opposing flows was the enhancement of the temperature gradient along the coast.

Temperature and wind profiles of individual stations indicated that the coastal front formed along the coastline of South Carolina yet developed over the interior coastal region of North Carolina and southern Virginia. These results alter the scope of the coastal front which previous studies indicated to be limited to the vicinity of the coast. However, these findings confirm previous results which rejected differential friction as a primary force in the frontogenesis process.

Convergence and positive relative vorticity patterns correlated well with the location of the coastal front while divergence and negative vorticity prevailed in the vicinity of the anticyclonic bulge. Observed deformation fields

indicated a favorable field for frontogenesis along the coastal region. On the contrary, geostrophic deformation fields were apparently associated with the anticyclonic bulge and had no relation to coastal frontogenesis.

Eulerian and Lagrangian surface frontogenesis fields were useful in confirming frontogenesis over the interior of North Carolina and southern Virginia. The confluence term of the Lagrangian calculations dominated the shear term, however, both the Lagrangian and Eulerian frontogenesis fields appeared to over-predict the increase of the temperature gradient. In part, the overestimation may be a result of the sub grid scale processes which do not allow the objective analysis scheme to accurately assess the true temperature gradient associated with the front.

Vertical cross sections through the frontal zone indicated a very shallow stable surface layer capped by a deeper layer of warmer air. At the transition zone from cold to warm air, the vertical temperature gradient was as large as 1 K per 20 meters. Three dimensional frontogenesis calculations revealed that horizontal confluence and shear terms were frontogenetical within the frontal zone while the tilting term was highly frontolytical within the frontal zone. Illustrations of wind components parallel and perpendicular to the front further define the front as a transition zone from northerly flow within the cold wedge to a stronger southerly flow which ascends over the dome from

the Atlantic.

A method of computing terrain level geostrophic winds was used to test the hypothesis that pressure reduction was responsible for the apparent ageostrophic flow within the cold wedge. Results based upon the terrain level wind faired only slightly better than the standard sea level geostrophic winds at predicting the cold wedge flow pattern.

This particular case study afforded an opportunity to view an unusual case of coastal frontogenesis. The inland development of the front appears to be an exception to the standard scenario. Further studies of coastal front events during the upcoming East Coast Cyclone Project (GALE) should attempt to obtain as much data on the vertical structure of the coastal front zone as is possible. Because this feature is so shallow, the rawinsonde observations of temperature and winds rarely contain more than two readings within the cold air dome. To obtain greater detail and better analyses, the rawinsondes should be adjusted to report several readings within the first 100 mb of the atmosphere. This detatiled information may allow future research to better relate vertical temperature and wind profiles to the evolution of the coastal front.

# Appendix A

## Derivation of Local Frontogenesis Equation in Cartesian Coordinates

As defined by Pettersen(1940), the local frontogenesis of any conservative property S, may be defined as

(1) $$F = \partial|\nabla S| / \partial t$$

For any vector

(2) $$|\nabla S| = (\nabla S \bullet \nabla S)^{.5}$$

Using the chain rule of differentiation, (1) becomes

(3) $$\partial|\nabla S| / \partial t = (1/2)(\nabla S \bullet \nabla S)^{-.5} * \partial(\nabla S \bullet \nabla S)/\partial t$$

$$= (1/(2\,|\nabla S|)) * \partial(\nabla S \bullet \nabla S)/\partial t$$

The rules of partial differentiation state

(4) $$\partial(A \bullet B)/\partial t = A \bullet \partial B/\partial t + \partial A/\partial t \bullet B$$

Applying (4) to complete the differentiation of the right hand side of (3) results in

$$\partial|\nabla S| / \partial t = 1/(2\,|\nabla S|) * 2\nabla S \bullet \partial|\nabla S| / \partial t$$

(5) $$= 1/(|\nabla S|) * \nabla S \bullet \partial|\nabla S| / \partial t$$

By definition of the total derivative and assuming the total derivative of a conservative property is equal to zero

(6) $$\partial|\nabla S| / \partial t = \nabla|\partial S| / \partial t = \nabla(-V \bullet \nabla S) + \nabla(dS/dt)$$

Substituting (6) into the right hand side of (5) yields

(7) $$\partial|\nabla S| / \partial t = (1/|\nabla S|) * \nabla S \; [\nabla(-V \bullet \nabla S) + \nabla(dS/dt)]$$

# REFERENCES

Ballentine, R. J., 1980: A numerical investigation of New England coastal frontogenesis. Mon. Wea. Rev., 108, 1479-1497.

Barnes, S. L., 1964: A technique for maximizing details in numerical weather map analysis. J. Appl. Meteor., 3, 396-409.

_____, 1973: Mesoscale objective map analysis using weighted time-series observations. NOAA Technical Memorandum ERL NSSL-62, Norman, OK, 60 pp.

Bergeron, T., 1937: On the physics of fronts. Bull. Amer. Meteor. Soc., 18, 265-275.

Bosart, L. F., C. J. Vaudo and J. H. Helsdon, Jr., 1972: Coastal frontogenesis. J. Appl. Meteor., 11, 1236-1258.

Bosart, L. F., and B. Korty 1976: coastal frontogenesis. Preprint of the First Conference of Coastal Meteorology, 47-54.

AD-A160 828 A CASE STUDY OF A MID-ATLANTIC COASTAL FRONT(U) AIR FORCE INST OF TECH WRIGHT-PATTERSON AFB OH J T KROLL 1985 AFIT/CI/NR-85-135T 2/2

UNCLASSIFIED F/G 4/1 NL

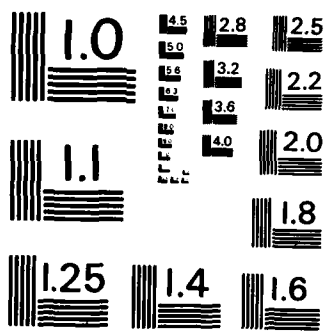


MICROCOPY RESOLUTION TEST CHART
NATIONAL BUREAU OF STANDARDS - 1963 - A

Bosart, L.F., 1975: New England coastal frontogenesis. Quart. J. Roy. Meteor. Soc., 101, 957-978.

_____, 1980: Coastal frontogenesis and cyclogenesis. Preprint of the Second Conference of Coastal Meteorology, 206-207.

_____, 1981: The president's day snowstorm of 18-19 February 1979: A subsynoptic scale event. Mon. Wea. Rev., 109, 1542-1566.

Bjerknes, J. 1919: On the structure of moving cyclones. Geofys. Publ., 1, 1-8.

_____, 1932: Explorations le quelques perturbations atmospherics a'l'aide de sondages rapproaches dans le temps. Geofys. Publ., 9, 52pp.

Carson, R. B., 1950: The Gulf Stream front: A cause of stratus on the lower Atlantic coast. Mon. Wea. Rev., 78, 91-100.

Doswell, C. A., 1984: A kinematic analysis of frontogenesis associated with a nondivergent vortex. J. Atmos. Sci., 41, 1242-1248.

Harms, D. E., 1985: Application of an objective analysis scheme to mesoscale observational network design. M.S. Thesis, NCSU, 91 pp.

Harrold, T. W., 1973: Mechanisms influencing the distribution of precipitation within baroclinic disturbances. Quart. J. Roy. Meteor. Soc., 99, 232-251.

Holton, J. R., 1979: An introduction to dynamic meteorology 2d ed. Academic Press, 391 pp.

Hoskins, B. J., 1971: Atmospheric frontogenesis models: Some solutions. Quart. J. Roy. Meteor. Soc., 97 , 139-153.

Koch, S. E., M. des Jardins and P. J. Kocin, 1981: The Gempak Barnes objective analysis scheme. NASA Technical Memorandum 83851 , NASA/GLAS, Greenbelt, MD, 56 pp.

Kreitzberg, C. W. and H. A. Brown, 1970: Mesoscale weather systems within an occlusion. J. Appl. Meteor., 9, 419-432.

Marks, F. D. and P. M. Austin, 1979: Effects of the New England coastal front on the distribution of precipitation. Mon. Wea. Rev., 107, 53-67.

Miller, J. E., 1948: On the concept of frontogenesis. J. Meteor., 5, 169-171.

Newton, C. W., 1954: Frontogenesis and frontolysis as a three-dimensional process. J. Meteor., 11, 449-461.

Palmen, E. and C. W. Newton, 1948: A study of the mean wind and temperature distribution in the vicinity of the polar front in winter. J. Meteor., 5, 220-226.

_____, 1969: Atmospheric Circulation systems. Academic Press , 603 pp.

Pettersen, S., 1940: Weather Analysis and Forecasting. McGraw-Hill, 505 pp.

_____, 1956: Weather Analysis and Forecasting, 2nd. ed., Vol. 1. McGraw-Hill, 428 pp.

Reed, R. J. and F. Sanders, 1953: An investigation of the development of a mid-troposperic frontal zone and its associated vorticity field. J. Meteor., 10, 338-349.

Reed, R. J. 1955: A study of a characteristic type of upper-level frontogenesis. J. Meteor., 12, 226-237.

Richwein, B. A., 1980: The domming effect of the southern Appalchians. Nat. Wea. Dig., 5, 2-12.

Sanders, F., 1955: An investigation of the structure and dynamics of an intense surface frontal zone. J. Meteor., 12, 542-552.

Sangster, W. E., 1960: A method of representing the horizontal pressure gradient force without the reduction of station pressures to sea level. J. Meteor., 17, 166, 176.

Saucier, W. J., 1955: Principles of Meteorological Analysis. University of Chicago, 438 pp.

_____, 1953: Horizontal deformation in atmospheric motion. Transactions, American Geophysical Union, 34, 709-719.

END

FILMED

12-85

DTIC